Available online at www.sciencedirect.com
ScienceDirect
Biochemical and Biophysical Research Communications 368 (2008) 501–507
BBRC
www.elsevier.com/locate/ybbrc

Nonhuman primate intestinal villous M-like cells: An effective poliovirus entry site ☆

Yoshihiro Takahashi [a,b], Shogo Misumi [b], Atsunobu Muneoka [a], Mitsuaki Masuyama [a,b], Hiroshi Tokado [a], Koichiro Fukuzaki [a], Nobutoki Takamune [b], Shozo Shoji [b,*]

[a] *Shin Nippon Biomedical Laboratories, Ltd., 2438 Miyanoura, Kagoshima 891-1394, Japan*
[b] *Department of Pharmaceutical Biochemistry, Faculty of Medical and Pharmaceutical Sciences, Kumamoto University, 5-1 Oe-Honmachi, Kumamoto 862-0973, Japan*

Received 11 January 2008
Available online 7 February 2008

Abstract

Humans and some Old World monkeys, chimpanzees, and cynomolgus macaques, are susceptible to oral poliovirus (PV) infection. Interestingly, rhesus macaques, although sensitive to injected PV, are not susceptible to gut infection. Not much is known about the initial event of gut infection by PV in rhesus macaques so far. Here, we show that PV can efficiently enter the lamina propria (LP) by penetrating across intestinal villous M-like cells in rhesus macaques. We found by immunofluorescence analysis that PV effectively invades LP rather than germinal centers (GCs) in rhesus macaques despite expressing PV receptor CD155 on cells within GCs and LP. Furthermore, energy dispersive X-ray spectroscopy demonstrated that gold-labeled PV is spatiotemporally internalized into villous M-like cells and engulfed by macrophage-like cells in LP. These results suggest that rhesus macaques may be resistant to productive gut PV infection owing to a defective translocation of PV to GCs.

Keywords: Villous M-like cell; Mucosa; Old World monkeys; Poliovirus; Gut infection

Nonhuman primates are the closest evolutionary relatives of humans. Their underlying physiology and metabolism, as well as genomic structure, are more similar to those in humans than to those in other mammals. This makes nonhuman primates particularly important as models of human diseases, including viral infectious diseases. Although chimpanzees are the animals most similar to humans, they are unsuitable for preclinical studies on ethical grounds because they are an endangered or threatened species. For other primates, there are the requirements of research utility and availability. Because of this, the rhesus and cynomolgus macaques are the excellent choice for pathophysiological and preclinical studies.

Humans are the only known natural hosts of poliovirus (PV), which causes poliomyelitis. In humans, PV has been isolated from tonsillopharyngeal tissues, the wall of the ileum, and mesenteric lymph nodes [1]. Oral PV infection can be associated with extensive tissue destruction in lymphoid organs of the pharynx, including the tonsils, and the small intestine, including Peyer's patches (PPs) [2], suggesting that the virus replicates in these tissues. In contrast, nonhuman primates are highly susceptible to PV via all routes except the oral route, yet some species show a certain degree of oral susceptibility [3]. Cynomolgus macaques are susceptible to infection via the oral route but only when a large dose of PV is administered. On the other hand, rhesus macaques are rarely susceptible to PV administered

Abbreviations: $CCID_{50}$, 50% cell culture infective doses; EDS, energy dispersive X-ray spectroscopy; FAE, follicle-associated epithelium; GCs, germinal centers; IFNAR, alpha/beta interferon receptor; LP, lamina propria; PV, poliovirus.

☆ The Ministry of Education, Culture, Sports, Science and Technology of Japan (16017287), and a Health Science Research Grant from the Ministry of Health, Labour, and Welfare of Japan (18220501).

* Corresponding author. Fax: +81 96 362 7800.
E-mail address: shoji@gpo.kumamoto-u.ac.jp (S. Shoji).

0006-291X/$ - see front matter © 2008 Elsevier Inc. All rights reserved.
doi:10.1016/j.bbrc.2008.01.120

orally. Iwasaki et al. suggested that in rhesus macaques, CD155 expression levels are low in the follicle-associated epithelium (FAE) and CD155 is not present in GCs [4]. In contrast, in humans, CD155 was detected on the intestinal epithelium, on M cells in PPs, and in GCs within PPs [4]. These findings suggest that PV replication in the gut may depend on the presence of CD155 in FAE, including M cells, and on cells in PPs. However, the gut infection pattern of PV using rhesus macaque models has not been performed so far.

CD155 transgenic (Tg) mice are also not susceptible to oral infection by PV [5,6]. CD155 is present at very low levels in the intestinal epithelium of these mice and absent in PPs [4,7]. Overexpression of CD155 in the intestinal epithelium of Tg mice induced by a fatty acid binding protein promoter also does not lead to oral susceptibility to PV [7]. Recently, Ohka et al. [8] detected PV in the epithelia of the small intestine, which proliferated in the alimentary tract of CD155 Tg mice lacking the alpha/beta interferon receptor (IFNAR) gene. These results suggest that IFNAR plays an important role in determining permissivity in addition to the appropriate expression of CD155 in the alimentary tract of Tg mice. However, this still has not explained why healthy humans and limited Old World monkeys are highly susceptible to gut PV infection despite robust innate immune responses including interferon signaling.

Whether human epithelial or immune cells are the primary sites of PV replication in the intestinal mucosa has remained unclarified as well. Although PV may easily gain access to the surface of FAE because it remains largely free from secretions such as mucus, glycocalyx or IgA, enterocytes other than those in the FAE may not be sufficiently accessible to PV to initiate infection. Furthermore, Iwasaki et al. indicated that the distribution of CD155 on human FAE-enterocytes other than M cells may not be favorable for intestinal PV infection because the distribution is higher on the basal side [4]. This notion is supported by the finding that M cells in humans are the site of PV penetration of the intestinal epithelial barrier [9]. From these results, we speculate that PV may not be preferentially absorbed into GCs through rhesus FAE-M cells and replicates in rhesus lymphoid tissues.

Typical FAE-M cells, characterized by an irregular brush border and a reduced amount of glycocalyx, efficiently take up and transport a wide variety of macromolecules and microorganisms from the gut lumen into PPs [10–14]. A recent study demonstrated that intestinal villous M cells serve as another antigen gateway in mice for the sampling of gut bacteria and subsequent induction of Ag-specific immune responses in a PPs-independent manner [15]. Thus, it is possible that villous M cells also serve as the PV entry site in the mucosal epithelium and are involved in oral PV infection in human and some Old World monkeys.

In this study, we discovered that, in rhesus macaques, PV can penetrate into LP via intestinal villous M-like cells rather than FAE-M cells, suggesting that rhesus macaques may be resistant to gut PV infection due to a defective translocation of PV to GCs via FAE-M cells.

Materials and methods

Animals and tissue samples. Purpose-bred female rhesus macaques (*Macaca mulatta*) obtained from a supplier in China (10–12 years old, weighing 4.55–6.26 kg) were used for this study. PPs of cynomolgus macaques (weighing 5–6 kg) were obtained from 4 to 5 years old female monkeys. This study (the Permission No. 19–137) was approved and carried out according to the guidelines of the Animal Care and Use Committee of Kumamoto University.

Gold labeling of PV. PV was labeled with gold colloid solution (5 nm, British BioCell International, Ltd.) according to the instruction manual. Gold nanoparticles not anchored on PV were readily removed by centrifugation. Gold-labeled PV was subjected to negative staining electron microscopy.

Inoculation of PV. Rhesus macaques were fasted overnight. They were then inoculated with 1 ml of PV solution (type 1, $10^{5.5}$–$10^{6.5}$ 50% cell culture infective doses ($CCID_{50}$); type II, $10^{4.5}$–$10^{5.5}$ $CCID_{50}$; type III, $10^{5.0}$–$10^{6.0}$ $CCID_{50}$) or 1 ml of gold-labeled PV at a site in the ileum (15 cm from the cecum) after celiotomy under anesthesia induced by a subcutaneous injection of urethane (ethyl carbamate, 800 mg/mL; 1.5 mL/kg body weight; Wako Pure Chemical Industries, Ltd.) solution and an intravenous injection of alpha-chloralose (Wako Pure Chemical Industries, Ltd.; 20 mg/mL; 5.5 mL/kg body weight) into the cephalic vein.

Collection of PPs. The rhesus monkeys were euthanized by exsanguination under anesthesia, and the part of the ileum (15 cm from cecum) including the inoculation site was collected. After washing the collected part of the ileum, 2 cm^2 blocks of PPs were fixed in ice-cold 3% glutaraldehyde/0.1 M sucrose/phosphate-buffered saline (pH 7.4). After 30 min of fixing, PPs were kept at 4 °C.

Histopathological study. Tissue samples were fixed in 10% neutral buffered formalin and were trimmed, embedded in paraffin, sectioned, stained with hematoxylin–eosin and examined by light microscopy.

Immunofluorescence staining. To examine the distribution of CD155 expression, the frozen sections of PPs were stained with various antibodies. In brief, 5 μm frozen sections were fixed in cold acetone and blocked with 1% nonfat skim milk in PBS(−). CD155 was detected using mAb D171 (Abcam Inc.) and FITC-conjugated anti-mouse IgG Ab, or FITC-labeled mouse mAb TX21 (MBL International). At the end of the staining, silides were wased and incubated with 4′,6-diamidino-2 phenylindole (DAPI) for nuclear staining (molecular Probes).

To examine how PV is incorporated into the lymphoid organ, the sections were stained with an anti-poliovirus antibody (II-MAP-01, Japan Poliomyelitis Research Institute) for 15 min. The sections were then incubated with TRITC-labeled goat anti-mouse IgG (Jackson Immunoresearch Laboratories) for 15 min. Finally, the sections were stained with FITC-labeled mouse mAb TX21. After the staining, slides were washed and analyzed with a Keyence Biozero BZ-8000.

Scanning electron microscopy (SEM). The tissue samples were rinsed in phosphate-buffered saline with 0.1 M sucrose (pH 7.4) and postfixed with 1% osmium tetroxide in 0.1 M phosphate buffer at 4 °C for 2 h. All the samples were dehydrated with 50:50, 70:30, 80:20, 90:10, and 95:5 ethanol/water mixtures and 100% ethanol for 10 min each and rinsed three times with 100% ethanol for further dehydration. The samples were critical-point dried by flooding with liquid carbon dioxide at 5 °C for 20 min and then raising the temperature to the critical-point (JCPD-5, JEOL). For SEM, samples were sputter-coated with gold (JFC-1100E, JEOL) and examined with a JEOL JSM-5200 scanning electron microscope at an accelerating voltage of 15 kV.

Transmission electron microscopy (TEM). The tissue samples were rinsed in phosphate-buffered saline with 0.1 M sucrose (pH 7.4) and postfixed with 1% osmium tetroxide in 0.1 M phosphate buffer at 4 °C for 2 h. All the samples were rinsed briefly with 50:50, 70:30, 80:20, 90:10, and 95:5 ethanol/water mixtures and 100% ethanol for 10 min each and three

times with 100% ethanol for dehydration, and then embedded in epoxy resin (Quatol 812). One micrometer sections were cut using a glass knife and then stained with toluidine blue. Suitable areas for ultrastructural study were chosen after examining 1 μm sections under a light microscope. Sections of 60–90 nm were cut on a Leica EM UC6 ultramicrotome using a diamond knife and sections were mounted on a copper grid and stained with 1% uranyl acetate and Reynolds lead citrate. The grids were examined under a JEOL JEM 1200-EX electron microscope.

Energy dispersive X-ray spectroscopy (EDS). EDS analysis, which was consigned to JEOL Datum Ltd., was performed to quantify PV by measuring gold concentration within a specimen.

Results

Intraintestinal inoculation site of PV in rhesus macaques

To elucidate the details of PV gut infection in rhesus macaques, an attenuated PV Sabin strain was carefully inoculated into the lumen of the ileum at 15 cm from the ileocecal valve (Fig. 1A). After inoculation, the terminal ileum tissue was subjected to light microscopy, immunofluorescence microscopy, SEM, and TEM. As shown in Fig. 1B, the largest Peyer's patch is found in the lumen of the terminal ileum in rhesus macaques. Light microscopy revealed the typical structure of a mucosal lymphoid follicle, composed of GCs and a dome area bulging into the lumen (Fig. 1C). Furthermore, SEM revealed that hemispherical domes were distributed between intestinal villi (Fig. 1D).

Comparison of CD155 expression in PPs between cynomolgus and rhesus macaques

To clarify the basis for the difference in susceptibility to oral PV infection between humans and rhesus macaques, Iwasaki et al. assessed the expression pattern of CD155 in PPs of these species. The results suggested that the suboptimal expression of CD155 in the rhesus macaque FAE and the lack of expression in GCs in PPs may explain why rhesus macaques are not susceptible to oral infection. Therefore, it is intriguing to speculate that in cynomolgus macaques, which are susceptible to oral PV infection, CD155 is most likely optimally expressed in FAE and GCs in PPs. To determine CD155 expression in cynomolgus macaques, we performed immunofluorescence staining of PPs using anti-CD155 Abs. The expression of CD155 in GCs in PPs was prominent in the case of staining with mAb D171 (Supplementary Fig. S1A) and mAb TX21 (Supplementary Fig. S1B) but that in FAE was not prominent. These results indicate that the mAbs used in this experiment can specifically stain CD155 on cells in cynomolgus GCs.

Furthermore, we assessed whether CD155 is not expressed in rhesus macaque PPs. Unexpectedly, in rhesus macaques, the expression level of CD155 on cells within FAE and GCs is not significantly different from that observed in cynomolgus macaques (Fig. 1E and F; see the less intensely stained GCs depicted by the DAPI nuclear staining in Fig. 1F). Furthermore, anti-CD155 mAb (TX21) can also stain cells in GCs in different sections of rhesus macaque PPs (Supplementary Fig. S1C).

Inoculated PV was efficiently incorporated into rhesus macaque villi

To examine how PV is incorporated into the lymphoid organ, attenuated PV was inoculated into the rhesus macaque ileum. One hour after the injection, the tissue was subjected to immunofluorescence analysis. As shown in Fig. 1H, the virus was detected inside the villi but was hardly detected in GCs that were strongly stained by anti-CD155 mAb (Fig. 1G). A merged image of panels 1G and 1H is shown in panel 1I. As shown in Fig. 1I, the colocalization of PV and CD155 was prominent in LP (Fig. 1I). When PPs from a different section were further observed, the virus was clearly detected in the LP of villi (Fig. 1J). On the other hand, weak fluorescence was detected in the subepithelial dome region in PPs (Fig. 1J) although fluorescence was hardly detected in GCs. These results indicate that PV efficiently enters into the villi rather than GCs within PPs in rhesus macaques. It is highly possible that a cofactor involved in PV accumulation in GCs is lacking in rhesus macaques.

SEM and TEM of FAE-M Cells

To examine why PV is not efficiently transported into cells in GCs underneath FAE, we investigated whether there are no typical M cells in rhesus macaque PPs because it has been suggested that PV is transported into PPs via human M cells [9]. Microscopy at a low magnification revealed hemispherical domes that were distributed between intestinal villi (Fig. 1K). Among cells in FAE, there were a few M cells showing a typical depressed surface with short and irregular microvilli (Fig. 1L). Rhesus macaque M-cell microvilli were shorter, thicker and fewer in number than the microvilli of adjacent absorptive enterocytes (Fig. 1M). Furthermore, the M-cell cytoplasm was invaginated by migrating lymphoid cells (Fig. 1M). These results demonstrated that there are typical M cells in rhesus macaque FAE, although we cannot exclude the possibility that rhesus macaque M cells in PPs cannot efficiently take up PV in comparison to human M cells.

SEM and TEM of villous M-like cells

To examine why PV is efficiently transported into LP, we investigated whether there are M-like cells in rhesus macaque villi because it has been demonstrated that intestinal villous M cells serve as a gateway for the antigen sampling of gut in mice [15]. SEM of rhesus macaque villous M-like cells revealed the hallmark feature of M cells, which is a typical depressed surface with short and irregular microvilli (Fig. 1N and O). TEM also showed villous M-like cells (Fig. 1P). Furthermore, infiltrating lymphocytes

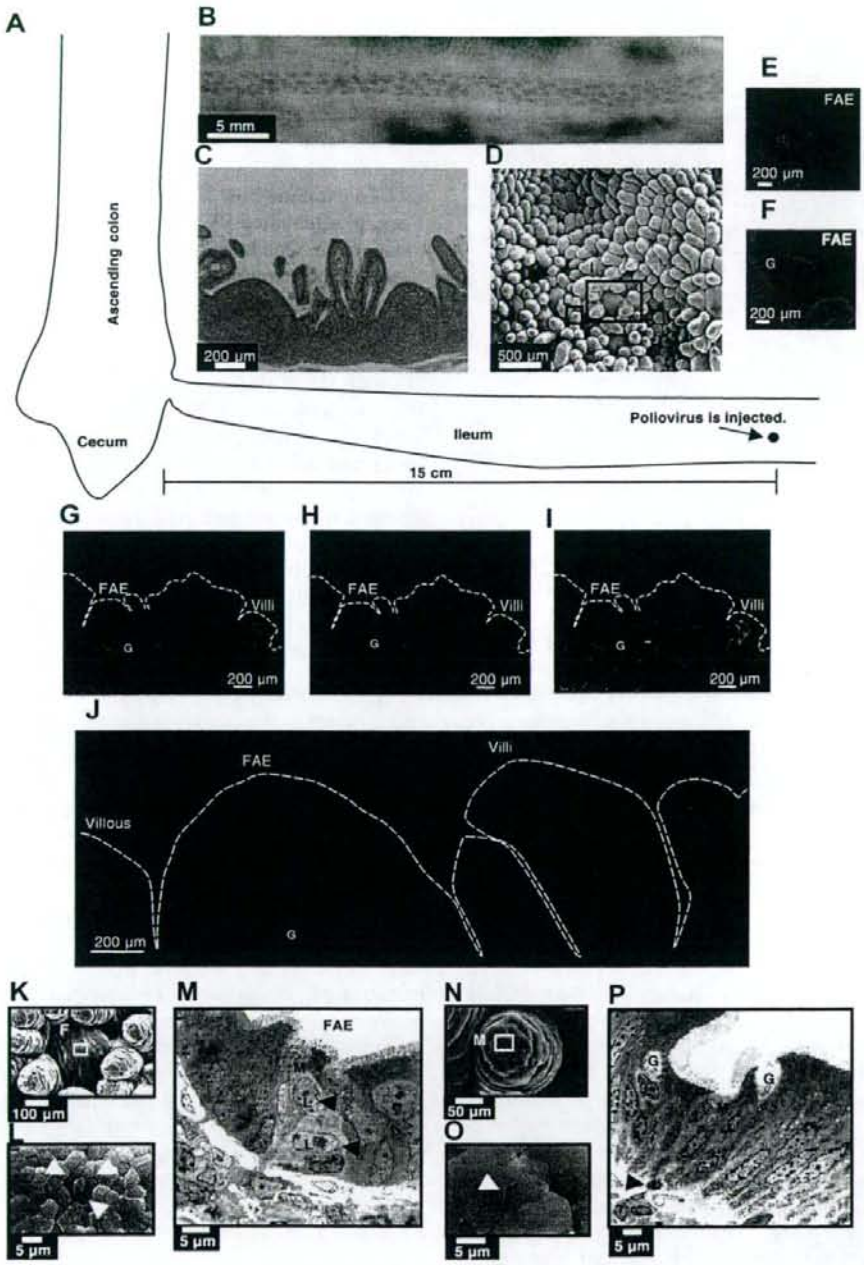

Fig. 1. PV is clearly detected in the lamina propria (LP) of villi. Attenuated PV was inoculated into the lumen of the ileum at 15 cm from the ileocecal valve (A). After inoculation, the parts of the ileum including the inoculation site and Peyer's patchs (PPs) were collected (B). Hematoxylin-eosin staining of rhesus PPs (C). Scanning-electron micrograph showing the ileum dome bulging into the gut lumen between intestinal villi (D). One hour after PV inoculation, the portion between the inoculation site of PV and the ileocecal valve was excised and subjected to immunofluorescence analysis. Frozen sections of rhesus macaque PPs were labeled with mAbs (D171 (E) and TX21 (G)) specific for CD155 (green) and nucleus was stained with 4', 6-diamidino-2 phenyindole (blue) (F). CD155 staining (G), PV staining (H), and merged (I) images are shown. (J) Different sections of rhesus macaque PPs were also stained by anti-PV mAb. PV can efficiently penetrate into the LP rather than into the subepithelial dome region. G, germinal center. SEM demonstrates that the M cells (K and L) in PPs and the villous M-like cells (N and O) in the villus epithelium are distinguishable from enterocytes by their relatively depressed and dark brush border (white arrowhead). TEM images of M cells in PP (M) and villous M-like cells in villi (P) show short stublike microvilli and the presence of infiltrating lymphocytes (L) in their pockets (black arrowhead). M, M cell or villous M-like cell.

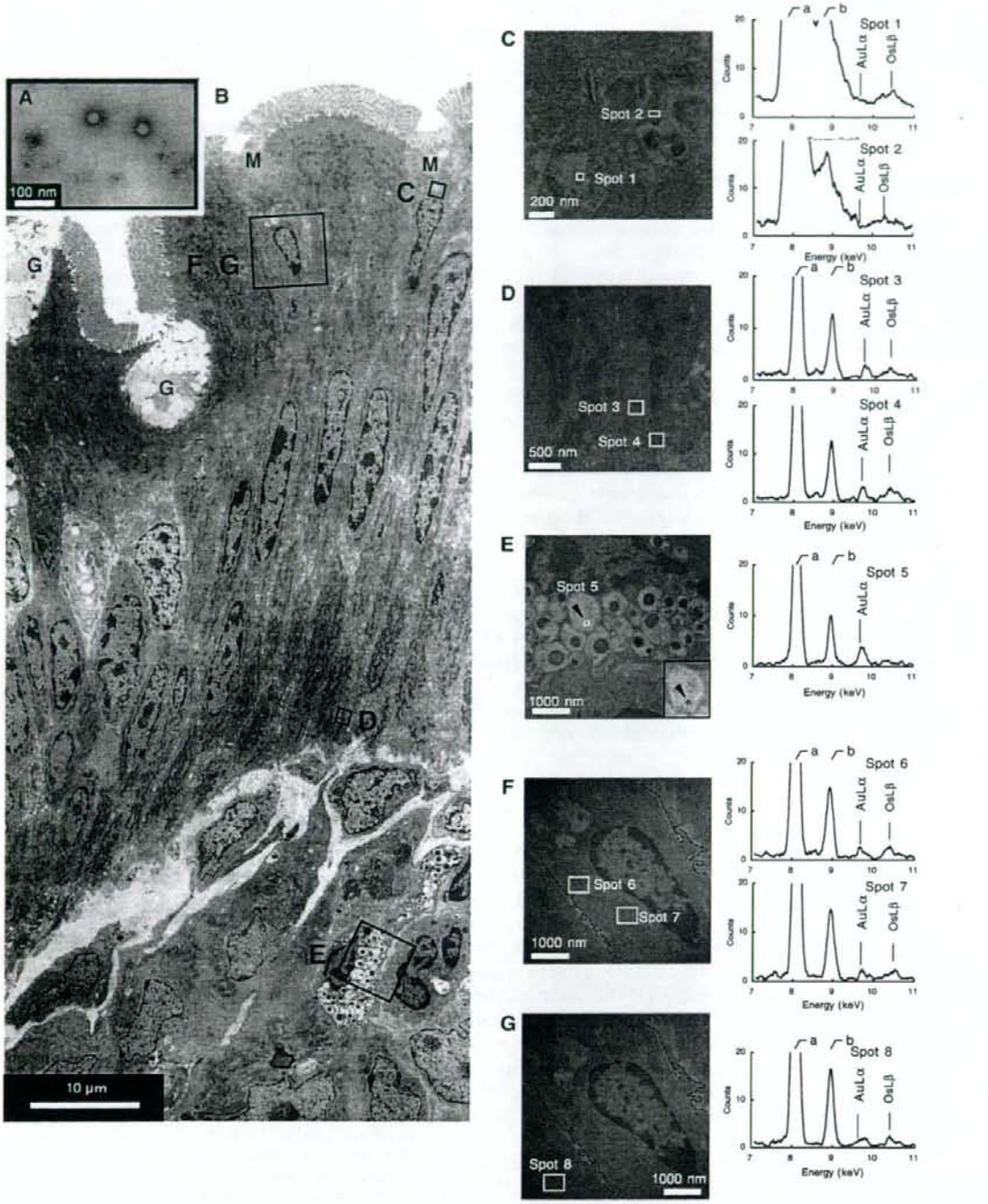

Fig. 2. PV can efficiently penetrate into villous M-like cells. PV was labeled with 5 nm gold particles and subjected to electron microscopies (A). A TEM view of villous epithelium (B) G, goblet cells; M, villous M-like cells. Panels (C–G) depict higher-magnification images of panel B for EDS. Graphs show EDS of spots (1–8) confirming the presence of gold particles (C–G). The a and b signals come from Cu (8.040 and 8.904 keV) that is attributed to the sample holder, and the b signal also contains the signal of OsLα (8.910 keV). The intensities of background signals from spots 1 and 2 in panel C were higher than those from other spots from panels D–G because spots 1 and 2 were on the TEM Cu-grid.

were also observed in the pockets of villous M-like cells (Fig. 1P). These results suggest that villous M-like cells may form an alternative gateway for PV and provide evidence that nonhuman primate M-like cells develop and localize in the villous epithelium as well as in the FAE of PPs.

Internalization of PV by villous M-like cells

To investigate whether rhesus macaque villous M-like cells can take up PV, the rhesus macaque ileum was inoculated with gold-labeled PV (Fig. 2A) and subjected to EDS. The advantage of EDS is that gold-labeled PV can be directly detected when PV is completely embedded in an ultrathin section. The characteristic X-ray peak from gold (AuL-alpha: approximately 9.712 keV) is used to confirm the presence of Nanogold within a section. Forty-five minutes after inoculation, EDS demonstrated the presence of gold-labeled PV in the basolateral cytoplasm (spots 3 and 4; Fig. 2B and D) but not in the apical cytoplasm (spots 1 and 2; Fig. 2B and C) of villous M-like cells. In addition, gold-labeled PV was also specifically engulfed by macrophage-like cells in LP (spots 5; Fig. 2B and E). As shown in the insert of Fig. 2E, a PV particle was clearly and directly detected. Furthermore, we examined whether the adjacent M-like cells also take up PV (spots 6 and 7; Fig. 2B and F). Results revealed the localization of PV beside the nucleus (Fig. 2F). In contrast, there is no signal corresponding to PV in an adjacent epithelial cell (spot 8; Fig. 2G). Taken together, these results indicate that rhesus macaque villous M-like cells have the ability to take up PV from the lumen.

Discussion

The premise of oral PV infection in humans postulates that CD155 is expressed not only on enterocytes in FAE but also on cells in GCs [4]. If so, cynomolgus epithelial cells in FAE and cells in GCs should express CD155 because cynomolgus macaques are susceptible to infection by PV administered orally. We searched for CD155 in PPs in cynomolgus macaques. Staining with CD155-specific mAbs (D171 and TX21) revealed that CD155 was highly expressed not only on enterocytes in FAE but also on cells in GCs.

However, not much has been known about the PV infection patterns in the gut of rhesus macaques so far. We examined whether CD155 is indeed not expressed within rhesus macaque GCs and whether PV is indeed not incorporated into rhesus macaque intestinal lymphoid tissue. Unexpectedly, staining with CD155-specific mAbs (D171 and TX21) revealed that rhesus macaque CD155 was highly expressed not only on cells in GCs but also on those in LP. Furthermore, our immunofluorescence analysis indicated that PV is efficiently incorporated into LP in the villi rather than into GCs. These findings suggest that in rhesus macaques, an as yet unidentified factor is required for the translocation of PV into GCs after PV penetrates into FAE-M cells, and that there are cells that function similarly to FAE-M cells as a gateway for PV on villi.

A recent study [15] has directly demonstrated the function of mouse villous M cells as a gateway for bacteria. The morphological characteristics of the rhesus macaque FAE-M cells in ileal PPs were previously reported [16], but to our knowledge, our present study is the first to show the function of nonhuman primate villous M-like cells as a gateway for PV. Rhesus macaque villous M-like cells were distinguishable from intestinal villous epithelial cells on the basis of the criteria including (i) short and irregular microvilli, (ii) endocytic activity and ability to take up PV as well as macromolecules, and (iii) an intraepithelial pocket that allows a cluster of lymphocytes to be located in the FAE of PPs; currently, there is no reliable identified antigen marker that can be used to positively identify primate villous M cells. Indeed, EDS analysis demonstrated that PV was internalized within villous M-like cells and transported into LP.

Acknowledgment

Both attenuated PV (Sabin Strain) and anti-PV Ab were obtained from the Japan Poliomyelitis Research Institute.

Appendix A. Supplementary data

Supplementary data associated with this article can be found, in the online version, at doi:10.1016/j.bbrc.2008.01.120.

References

[1] A.B. Sabin, R. Word, The natural history of human poliomyelitis: I. Distribution of virus in nervous and non-nervous tissues, J. Exp. Med. 73 (1941) 771–793.
[2] D. Bodian, Emerging concept of poliomyelitis infection, Science 122 (1955) 105–108.
[3] G.D. Hsiung, B.D. Black, J.R. Henderson, Susceptibility of primates to viruses in relation to taxonomic classification, in: J. Buettner-Janusch (Ed.), Evolutionary and Genetic Biology of Primates, vol. II, Academic Press, New York, NY, 1964, pp. 1–23.
[4] A. Iwasaki, R. Welker, S. Mueller, M. Linehan, A. Nomoto, E. Wimmer, Immunofluorescence analysis of poliovirus receptor expression in Peyer's patches of humans, primates, and CD155 transgenic mice: implications for poliovirus infection, J. Infect. Dis. 186 (2002) 585–592.
[5] S. Koike, C. Taya, T. Kurata, S. Abe, I. Ise, H. Yonekawa, A. Nomoto, Transgenic mice susceptible to poliovirus, Proc. Natl. Acad. Sci. USA 88 (1991) 951–955.
[6] R.B. Ren, F. Costantini, E.J. Gorgacz, J.J. Lee, V.R. Racaniello, Transgenic mice expressing a human poliovirus receptor: a new model for poliomyelitis, Cell 63 (1990) 353–362.
[7] S. Zhang, V.R. Racaniello, Expression of the poliovirus receptor in intestinal epithelial cells is not sufficient to permit poliovirus replication in the mouse gut, J. Virol. 71 (1997) 4915–4920.
[8] S. Ohka, H. Igarashi, N. Nagata, M. Sakai, S. Koike, T. Nochi, H. Kiyono, A. Nomoto, Establishment of a poliovirus oral infection system in human poliovirus receptor-expressing transgenic mice that are deficient in alpha/beta interferon receptor, J. Virol. 81 (2007) 7902–7912.

[9] P. Sicinski, J. Rowinski, J.B. Warchol, Z. Jarzabek, W. Gut, B. Szczygiel, K. Bielecki, G. Koch, Poliovirus type 1 enters the human host through intestinal M cells, Gastroenterology 98 (1990) 56–58.
[10] A. Frey, K.T. Giannasca, R. Weltzin, P.J. Giannasca, H. Reggio, W.I. Lencer, M.R. Neutra, Role of the glycocalyx in regulating access of microparticles to apical plasma membranes of intestinal epithelial cells: implications for microbial attachment and oral vaccine targeting, J. Exp. Med. 184 (1996) 1045–1059.
[11] J.P. Kraehenbuhl, M.R. Neutra, Epithelial M cells: differentiation and function, Annu. Rev. Cell Dev. Biol. 16 (2000) 301–332.
[12] M.R. Neutra, A. Frey, J.P. Kraehenbuhl, Epithelial M cells: gateways for mucosal infection and immunization, Cell 86 (1996) 345–348.
[13] M.R. Neutra, N.J. Mantis, A. Frey, P.J. Giannasca, The composition and function of M cell apical membranes: implications for microbial pathogenesis, Semin. Immunol. 11 (1999) 171–181.
[14] R.L. Owen, Sequential uptake of horseradish peroxidase by lymphoid follicle epithelium of Peyer's patches in the normal unobstructed mouse intestine: an ultrastructural study, Gastroenterology 72 (1977) 440–451.
[15] M.H. Jang, M.N. Kweon, K. Iwatani, M. Yamamoto, K. Terahara, C. Sasakawa, T. Suzuki, T. Nochi, Y. Yokota, P.D. Rennert, T. Hiroi, H. Tamagawa, H. Iijima, J. Kunisawa, Y. Yuki, H. Kiyono, Intestinal villous M cells: an antigen entry site in the mucosal epithelium, Proc. Natl. Acad. Sci. USA 101 (2004) 6110–6115.
[16] E.M. Kuhn, F.J. Kaup, Morphological characteristics of the ileal Peyer's patches in the rhesus macaque: a histological and ultrastructural study, Anat. Histol. Embryol. 25 (1996) 65–69.

Biochemical and Biophysical Research Communications 377 (2008) 617–621

Contents lists available at ScienceDirect

Biochemical and Biophysical Research Communications

journal homepage: www.elsevier.com/locate/ybbrc

Development of cell-expressed and virion-incorporated CCR5-targeted vaccine ☆

Shogo Misumi [a,*], Ayumi Eto [a], Ryotarou Mitsumata [a], Masanori Yamada [a], Nobutoki Takamune [a], Shozo Shoji [a,b]

[a] Department of Pharmaceutical Biochemistry, Faculty of Medical and Pharmaceutical Sciences, Kumamoto University, 5-1 Oe-Honmachi, Kumamoto 862-0973, Japan
[b] Kumamoto Health Science University, Kumamoto 861-5598, Japan

ARTICLE INFO

Article history:
Received 6 October 2008
Available online 16 October 2008

Keywords:
Cell-expressed CCR5
Virion-incorporated CCR5
Cycloimmunogen
SIV_{mac239}

ABSTRACT

Our previous study demonstrated that the immunization with a cycloimmunogen derived from extracellular loop-2 (ECL-2) of CCR5 (cDDR5) attenuated acute phase of CCR5-tropic simian-human immunodeficiency virus $(SHIV)_{SF162P3}$ replication *in vivo*. Although the study showed that the antisera raised against cDDR5 reacted with cell-expressed CCR5, we have not yet demonstrated whether the antisera can react with virion-incorporated CCR5. Here, we show that rhesus cDDR5 (rcDDR5)-specific antibodies react with not only cell-expressed but also virion-incorporated simian CCR5s (siCCR5s), but may predominantly exert their inhibitory effects on simian immunodeficiency virus (SIV) infection by the binding of cell-expressed rather than virion-incorporated CCR5s. These results suggest that the virion-incorporated CCR5 may contribute to the reactivation of the anti-rcDDR5 antibody-producing B-cells by SIV particles after rcDDR5 immunization, although the binding of anti-rcDDR5 antibody to virion-incorporated CCR5 results in a partial inhibitory effect on SIV infection.

The human immunodeficiency virus (HIV) uses cell-surface receptors to gain entry into target cells. CD4 is the main receptor, and a chemokine receptor CCR5 is the coreceptor utilized by CCR5-tropic (R5) viruses. CXCR4, an alternative chemokine receptor, is used by CXCR4-tropic viruses. The distribution of these receptors is critical for HIV transmission and infection. In fact, the most striking resistance to HIV infection is in the naturally occurring delta32 CCR5 mutation in approximately 1% of Caucasians [1,2]. These individuals lack the cell-surface expression of CCR5. Furthermore, some studies showed that mucosal antibody responses may contribute to the apparent resistance to HIV-1 infection. The studies, in which humoral responses against HIV-1 in the vaginal secretions of women who remain uninfected despite frequent unprotected sex with HIV-1-infected partners were analyzed, indicated the presence of CCR5-specific mucosal autoantibodies [3].

As attempts to reproduce some of the functional aspects of the natural resistance to HIV infection, some vaccination strategies of inducing CCR5-specific autoantibodies have been reported. Our previous attempts were to induce CCR5-specific autoantibodies with anti-R5 HIV-1 activity by the inoculation of cDDR5 from the UPA (from Arg_{168} to Cys_{178}) of ECL-2 in CCR5 into Balb/c mice [4] and cynomolgus macaques [5]. Other attempts include the induction of CCR5-specific autoantibodies with anti-R5 HIV-1 activity by the inoculation of recombinant papillomavirus-like particles, which represent an extracellular loop of CCR5, into C57BL/6 mice and pig-tail macaques [6,7], and by the immunization of rhesus macaques with synthetic linear peptides (*N*-terminal peptide $_{1-20}$, first-loop $peptide_{89-102}$, and second-loop $peptide_{178-197}$) derived from the *N*-terminus, first loop, and second loop in CCR5 [8]. Results of these studies indicate that vaccines aimed at inducing CCR5-specific autoantibodies can be developed to reproduce some of the functional aspects of this natural resistance by blocking and down-modulating the CCR5 on the surface of HIV-targeted cells, as well as conventional viral-protein-based vaccines.

A recent intriguing study by Yusa and coworkers [9] has suggested that CCR5 is incorporated into HIV virions. Depending on the surface of the host cell, HIV-1 incorporates cell-derived molecules into its envelope [10,11]. Previous studies showed that HLA-class I, CD54, and other cellular surface proteins were incorporated into a budding virion [12], whereas CD4, CXCR4, and CCR5 were not detectable [13]. However, Yusa and coworkers found that CCR5 is incorporated into budding virions using the various types of monoclonal antibodies against the cell-surface molecules. The

Abbreviations: SHIV, simian-human immunodeficiency virus ECL-2, extracellular loop-2 siCCR5, simian CCR5 SIV, simian immunodeficiency virus UPA, undecapeptidyl arch HIV, human immunodeficiency virus R5, CCR5-tropic

☆ Funding: Ministry of Education, Culture, Sports, Science and Technology of Japan (16017287), and a Health Science Research Grant from the Ministry of Health, Labour, and Welfare of Japan (18220501).

* Corresponding author. Fax: 81 96 362 7800.
E-mail address: misumi@gpo.kumamoto-u.ac.jp (S. Misumi).

0006-291X/$ - see front matter © 2008 Elsevier Inc. All rights reserved.
doi:10.1016/j.bbrc.2008.10.022

result suggests that CCR5-specific autoantibodies induced by vaccines may be capable of not only blocking and down-modulating the CCR5 on the surface of HIV-targeted cells but also directly neutralizing HIV infection.

In this study, we suggest that siCCR5 is incorporated into SIV_{mac239} particles, and cDDR5 derived from ECL-2 of siCCR5 is an attractive mimotope for inducing anti-siCCR5 antibodies against cell-expressed and virion-incorporated siCCR5s.

Materials and methods

Preparation of SIV_{mac239} lysate. The supernatants from the culture media of SIV_{mac239}-infected HSC-F cells [14] and rhesus peripheral blood mononuclear cells (PBMCs) were filtered through a 0.45 μm disposable filter and then centrifuged at 43,000g for 3 h at 4 °C. The pellet was resuspended in PBS(−) and then centrifuged at 100,000g for 1 h at 4 °C. The resulting pellet and SIV_{mac239}-infected HSC-F cells were lysed in 200 μl of lysis buffer (125 mM Tris–HCl (pH 6.8) containing 4% SDS and 20% glycerol).

Sodium dodecyl sulfate–polyacrylamide gel electrophoresis (SDS–PAGE) and western immunoblot analysis. The diluted lysate was separated by sodium dodecyl sulfate–polyacrylamide gel electrophoresis (SDS–PAGE) [15] (PAG Mini "DAIICHI" 4–20%, Daiichi Pure Chemicals, Tokyo, Japan) and the separated proteins were subsequently electroblotted onto a polyvinylidene difluoride membrane (Immobilon, Millipore Corporation, Bedford, MA, USA). Antigens were probed with anti-siCCR5 antibody, 3A9 (BD Biosciences), and murine anti-SIV_{mac251} gp130 monoclonal antibody (Immuno Diagnostic Inc.). The bands were visualized by chemiluminescence detection (NEN Life Science Products, Boston, MA, USA).

Preparation of rhesus CCR5-derived cDDR5-keyhole limpet hemocyanin (KLH). A siCCR5-derived linear dodecapeptide (linear rhesus DDR5, H_2N-DRSQREGLHYTG-COOH), in which all side-chain groups are protected, was synthesized using an automatic peptide synthesizer and cyclized, as previously described [4]. The molecular masses of rhesus macaque CCR5-derived cDDR5 (rcDDR5) were determined by MALDI-TOF-mass spectrometry (Burker Franzen Analytik). The gamma-carboxyl group of Glu_1 in the protected rcDDR5 was conjugated to ethylenediamine and then coupled to KLH through Bis(sulfosuccinimidyl)suberate (Thermo Fisher Scientific Inc.).

Immunization and screening. Ten BALB/c mice were immunized intraperitoneally with 200 μg of rcDDR5-KLH in Freund's adjuvant at 1-week intervals and administered an intravenous boost of 40 μg of rcDDR5-KLH 3 days prior to splenectomy. Eleven hybridomas were generated by a standard method, by which splenocytes were fused with P3U1 cells and selected in hypoxanthine-, aminopterin-, and thymidine-supplemented media. In the screening, supernatants were tested for reactivity to rcDDR5-Multi-Pin Block in accordance with the method described in Ref. [4]. Hybridomas that produced high titers of anti-rcDDR5 antibodies (MARS4 and MARS8) were then cloned. MARS4 and MARS8 were found to be monoclonal and immunoglobulin G_3 and G_{2a} isotypes, respectively.

Flow cytometry. HSC-F cells were preincubated with or without MIP-1beta (1 ng) at 37 °C for 30 min. These cells were washed with a washing buffer (phosphate-buffered saline (PBS) containing 2% fetal calf serum and 0.02% NaN_3), and then stained with MARS4 at 4 °C for 30 min. These cells were washed with a washing buffer, and FITC-conjugated anti-mouse IgG was used for antibody staining. After 30 min of incubation at 4 °C, the cells were washed and then analyzed using an EPICS XL flow cytometer (Beckman Coulter).

Chemotaxis assay. A chemotaxis assay was performed using the protocol of Gosling et al. [16] with HSC-F cells (5×10^5 cells) treated with or without MARS8. The assay was conducted in the presence of 10 ng/ml MIP-1beta placed in the lower chamber. Transwells (pore size, 5 μm; Corning Inc., Corning, NY) were incubated for 5 h at 37 °C. The cells that migrated from the upper chamber to the lower chamber were quantified by trypan blue dye exclusion.

Virus-binding ELISA. The pellet of the purified SIV_{mac239} (50 ng of p27 antigen) was suspended in anti-rcDDR5 serum, normal mouse serum, 1 μg of antibodies to SIV ENV protein (murine anti-SIV_{mac251} gp130 monoclonal antibody (Immuno Diagnostic Inc.)), or to siCCR5 (3A9, BD Biosciences), then incubated on ice for 30 min, and washed with PBS(−). The resulting viral pellet was resuspended with 50 μl of protein G microBeads (Miltenyi Biotec), incubated on ice for 30 min, and washed with 200 μl of PBS(−). The immune complex of antibody–virus–protein G microBeads was purified in accordance with the manufacturer's instructions, and lysed with 20 μl of 95 °C-prewarmed lysing buffer in Retro-Tek SIV p27 Antigen ELISA kit (ZeptoMetrox Corporation) for 5 min. The lysate was eluted with 50 μl of elution buffer (lysing buffer:PBS(−)=1:9) before quantification of p27 by ELISA.

Total viral DNA detection assay. To evaluate the inhibitory effect of MARS4, the HSC-F cells (1×10^6 cells) or SIV_{mac239} was pretreated in the following three different ways with MARS4. (Cell block) HSC-F cells were preincubated with MARS4 for 30 min and then washed. The cells were then incubated with SIV_{mac239} (50 ng of p27 antigen) in the presence of DEAE dextran (20 μg/ml) for 4 h, washed twice with the culture medium, and cultured in fresh medium (200 μl) for 40 h. (Virus block) SIV_{mac239} was preincubated with MARS4 for 30 min and then washed by centrifugation (100,000g). The virus was incubated with HSC-F cells in the presence of DEAE dextran for 4 h. Finally, the HSC-F cells were washed twice with the culture medium and cultured in fresh medium (200 μl) for 40 h. (Cell/virus block) HSC-F cells were preincubated with MARS4 for 30 min. Without washing, the cells were then incubated with SIV_{mac239} (50 ng of p27 antigen) in the presence of MARS4 and DEAE dextran (20 μg/ml) for 4 h, washed twice with the culture medium, and cultured in fresh medium (200 μl) for 40 h. After this, the HSC-F cells were harvested. The nucleic acid obtained after the purification procedure [17] was used for the PCR amplification. cDNA duplicates were amplified by SYBR green real-time PCR assay as previously described [18] with some modifications. Briefly, primers that recognize specific and highly conserved sequences on the *gag* region of SIV described by Ui et al. [19] were selected. The sequences of SIV *gag* primers were 5′-GGAAATTACCCAGTACAACAAATAGG-3′ and 5′-TCTATCAATTTTACCCAGGCATTTA-3′. The SIV *gag* gene was amplified in 20 μl of a PCR mixture consisting of 10 μl of 2× master mix containing modified DyNAmo hot start DNA polymerase, SYBR green I, optimized PCR buffer, 5 mM $MgCl_2$, a dNTP mix including dUTP (Finnzymes), 2 μl of each primer, and 8 μl of viral DNA. PCR was conducted as follows: initial activation of hot start DNA polymerase at 95 °C for 15 min; 40 cycles of four steps of 95 °C for 10 s, 57 °C for 20 s, 72 °C for 20 s, and 76 °C for 2 s. At the end of the amplification cycle, melting temperature analysis was conducted by gradually increasing the temperature (0.5 °C/s) to 95 °C. Amplification, data acquisition, and analysis were conducted with the DNA Engine Opticon 2 System (Bio-Rad Laboratories Inc.) using Opticon Monitor version 2.02 software (Bio-Rad Laboratories Inc.).

Results

Incorporation of siCCR5 into SIV_{mac239}

To examine the incorporation of siCCR5 into the envelope of SIV_{mac239}, the lysates from viruses grown in either HSC-F or rhesus PBMC were subjected to western immunoblot analysis with anti-siCCR5 antibody, 3A9 (Fig. 1A and B), and murine anti-SIV_{mac251} gp130 monoclonal antibody that cross-reacted with SIV_{mac239} Env protein (Fig. 1C and D). Consistent with other reports [20,21], a band corresponding to siCCR5 monomer was detected in both

cases, which migrated with an apparent 48 kD mass (Fig. 1A and B). Furthermore, higher-molecular-weight species as shown in Refs. [20,21] were also detected in SIV_{mac239} from rhesus PBMC (Fig. 1B) but not from HSC-F cells that predominantly expressed CCR5 having a molecular weight of approximately 48 kDa (Fig. 1A). As a positive control, anti-SIV_{mac251} gp130 monoclonal antibody was used, which detected SIV_{mac239} Env protein in both cases (Fig. 1C and D). Although supernatants from uninfected cells as a negative control were also subjected to western immunoblot analysis, a band corresponding to siCCR5 was not detected (data not shown).

rcDDR5 synthesis and peptide analysis

It is generally considered that the conformational B-cell epitopes involved in the induction of a conformation-specific antibody would be difficult to mimic using a simple synthetic linear peptide. To mimic the UPA of ECL2 of rhesus CCR5, a linear side-chain group-blocked oligopeptide (linear rhesus DDR5 (rDDR5): H_2N-ERSQREGLHYTG-COOH) with a free-amino-terminal head and a carboxyl-terminal tail was first synthesized and then cyclized by peptidyl bond formation between the amino group of Glu_1 and the carboxyl group of Gly_{12} (Fig. 2A). After the removal of the side-chain-blocking group, rcDDR5 (cyclized at the head and tail of linear rDDR5) was purified, and its molecular masses was determined by MALDI-TOF-MS using alpha-cyano-4-hydroxy-cinnamic acid as a matrix. The spectrum of purified rcDDR5 exhibited major peaks at m/z 1414.66 (Fig. 2B), suggesting that the structure of rcDDR5 is cyclo($ER_{168}S_{169}Q_{170}R_{171}E_{172}G_{173}L_{174}H_{175}Y_{176}T_{177}G$).

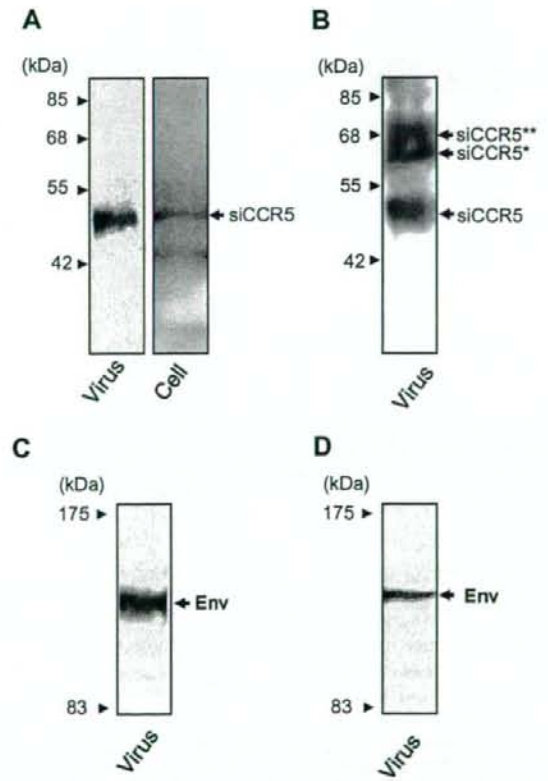

Fig. 1. Incorporation of siCCR5 into SIV_{mac239}. Viral lysates (2 μg) produced from HSC-F or rhesus PBMCs were resolved by 4–20% SDS–PAGE. Western immunoblot analysis was performed using anti-siCCR5 antibody, 3A9 (A and B), and murine anti-SIV_{mac251} gp130 monoclonal antibody (C and D). Furthermore, the cell lysate of HSC-F cells was also subjected to western immunoblot analysis using 3A9 for comparison (A).

Immunochemical specificity of the anti-rcDDR5-MAP antibodies, MARS4 and MARS8

Among the many antibody-producing clones, two clones producing the antibody to rcDDR5-KLH was effectively selected using the rcDDR5-Multi-Pin Block. The novel monoclonal antibodies, MARS4 and MARS8 (IgG_3 and IgG_{2a} isotypes, respectively) were selected (Fig. 2C). The immunochemical specificities of MARS4 and MARS8 were determined using flow cytometry (Fig. 2D) and chemotaxis assay (Fig. 2E). MARS4 was bound to CCR5-expressing HSC-F cells (Fig. 2D) but the binding was significantly competed with MIP-1beta (Fig. 2D). Furthermore, MARS8 significantly interfered with the chemotaxis induced by MIP-1beta (Fig. 2E). These results suggest that rcDDR5 immunization can induce the anti-siCCR5 antibody.

Binding of anti-rcDDR5 serum to virion-incorporated siCCR5

To examine whether anti-rcDDR5 serum from mice immunized with rcDDR5-KLH can recognize the virion-incorporated siCCR5, we measured the amount of intact SIV_{mac239} particles captured by anti-rcDDR5 serum using a virus-binding ELISA as shown in "Materials and Methods". SIV_{mac239} particles were treated with anti-rcDDR5 serum or normal mouse sera. Alternatively, both the commercially available anti-siCCR5 antibody, 3A9 and the anti-SIV ENV protein antibody were also used as controls. As expected, the anti-rcDDR5 serum captured the SIV_{mac239} grown in HSC-F cells (Fig. 3A). As a positive control, the anti-SIV ENV protein antibody effectively captured the HSC-F cell-derived virions, and 3A9 also captured the virions although the binding efficiency of 3A9 to siCCR5 was lower than that of the anti-rcDDR5 serum. These results suggest that the UPA is an attractive target for immune strategies aimed at generating anti-CCR5 antibodies.

Antiviral activity

Because siCCR5 is the main coreceptor for SIV_{mac239} and is incorporated into the SIV_{mac239} envelope, we investigated whether MARS4 could inhibit SIV_{mac239} entry via cell-expressed or virion-incorporated CCR5. The anti-SIV_{mac239} activities of MARS4 were determined using HSC-F cells that express CCR5 and SIV_{mac239} grown in HSC-F cells. The pretreatment of cells with MARS4 resulted in a significant inhibitory effect on SIV_{mac239} infection (Fig. 3B). On the other hand, the pretreatment of the virus with MARS4 resulted in a partial inhibitory effect on SIV_{mac239} infection (Fig. 3B). Furthermore, when MARS4-pretreated cells were inoculated with SIV_{mac239} in the presence of MARS4, it resulted in the most effective inhibitory effect (Fig. 3B). These results suggested that the rcDDR5-induced anti-CCR5 antibody may effectively show inhibitory effects through the binding to the cell-expressed rather than virion-incorporated CCR5s.

Discussion

Could CCR5 be an attractive target for the development of HIV vaccines? Persons with the homozygous delta32 CCR5 mutation, a 32-base-pair deletion of the CCR5 gene that results in a lack of cell-surface expression of CCR5, have strongly reduced susceptibility to CCR5-dependent HIV-1 infection [1,22,23]. Furthermore, Pastori et al. found that long-lasting CCR5 internalization by anti-CCR5 antibodies in a subset of long-term nonprogressors is associated

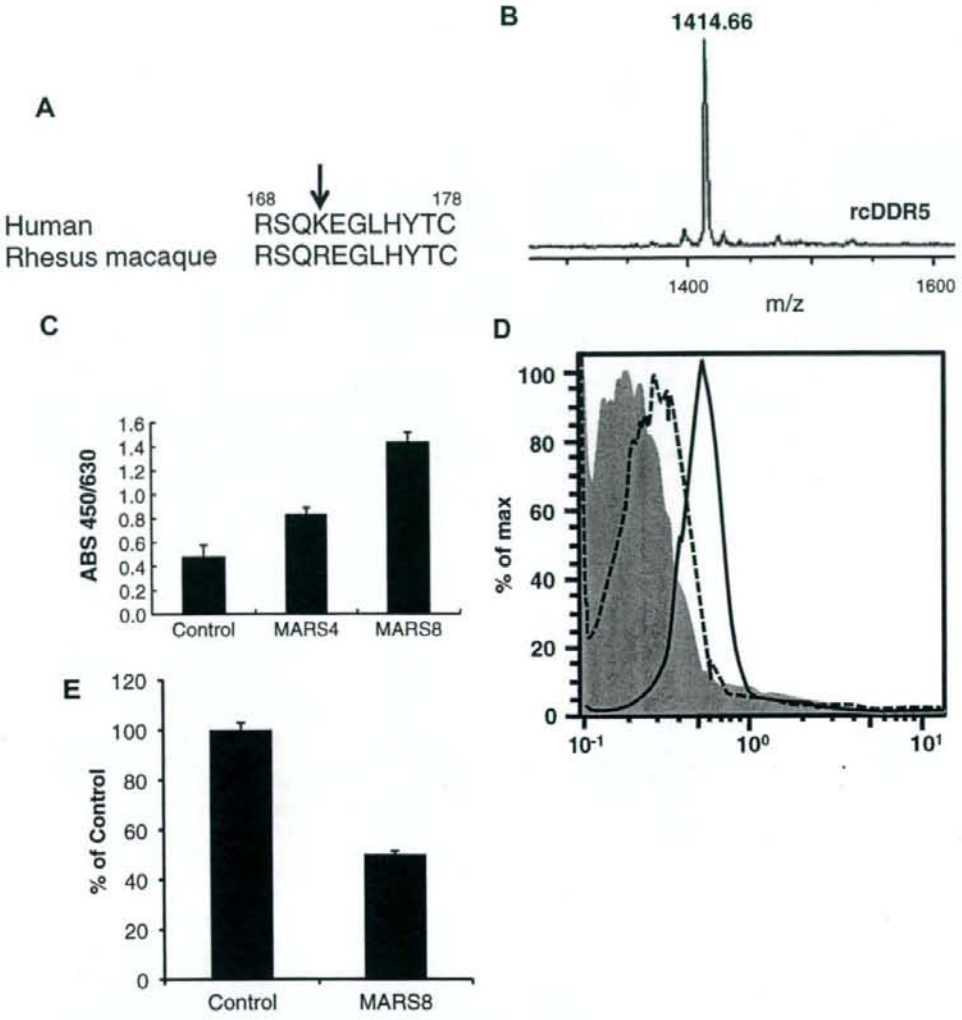

Fig. 2. Cloning of anti-rcDDR5 antibodies, MARS4 and MARS8, and their specificities. (A) Difference in UPA sequence between human and rhesus macaque. (B) MALDI-TOF-MS spectrum of rcDDR5. The spectrum exhibited a peak at *m/z* 1414.66. (C) Screening of anti-rcDDR5 antibodies, MARS4 and MARS8, using rcDDR5-Multi-Pin ELISA as described in "Materials and methods." (D) MARS4 binds specifically to siCCR5 on the cell surface. HSC-F cells were exposed to MARS4 in the absence (dotted line) or presence (bold line) of MIP-1beta or in the presence of an isotype-matched control antibody (gray shadow) at 4 °C. (E) MARS8 interferes with MIP-1beta-induced THP-1 chemotaxis. Results are expressed in terms of % of control, which represents the number of cells migrating in response to MIP-1beta over the number of cells migrating spontaneously in the control medium multiplied by 100.

with a possible protective effect against disease progression [24], suggesting that the induction of anti-CCR5 antibodies by a vaccine could reproduce the immune status in long-term nonprogressors. Thus, these data make CCR5 an attractive potential target for the development of HIV vaccines.

In general, it is considered that antibodies neutralize enveloped viruses by diverse mechanisms, such as disruption of receptor binding, interference with conformational changes required for virus entry, steric hindrance, or virus aggregation [25,26]. We previously showed that the antisera raised against cDDR5 mimicking the UPA of human CCR5 reacted with human CCR5, and potently suppressed infection by the R5 HIV-1 isolates [4,5], suggesting that HIV infection can be neutralized by the anti-CCR5 antibody-mediated interference with receptor binding of the envelope glycoproteins. Recently, Yusa and coworkers found that CCR5 is incorporated into budding virions [9]. The result suggests that CCR5-specific antibodies induced by vaccines may be capable of not only blocking the CCR5 on the surface of HIV-targeted cells but also directly neutralizing HIV infection. In this study, the immunization with rcDDR5-conjugated KLH induces anti-rcDDR5-specific monoclonal IgGs and anti-rcDDR5 serum that specifically bind to both the cell-expressed and virion-incorporated siCCR5s. Although the antibody binding to virion-incorporated CCR5 had a potential to inhibit SIV_{mac239} infection, only partial inhibition was observed. These results suggest that the rcDDR5-induced antibody binding to cell-expressed CCR5 may predominantly establish a steric block to a step in the virus entry process rather than that to virion-incorporated CCR5.

The incorporation of CCR5 in virions raises another hypothesis that the anti-CCR5 antibody can be simultaneously induced

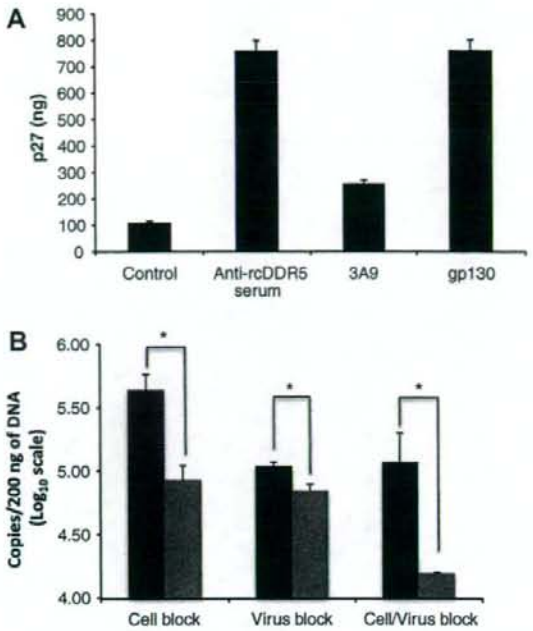

Fig. 3. Reactivity of anti-rcDDR5 serum to siCCR5 on the SIV_{mac239} envelope and the antiviral activity of MARS4. (A) The capture of SIV_{mac239} by anti-rcDDR5 serum was determined by a virus-binding ELISA as described in "Materials and methods". (B) The antiviral activity was measured as described in "Materials and methods". Each control experiment was carried out without MARS4 pretreatment. Results represent the amount of viral DNA (copies/200 ng of DNA) in each sample pretreated with MARS4 (gray column) or in each control sample (black column). $^{*}P<0.05$ by Mann–Whitney *U*-test.

when HIV invades the human body after cDDR5 immunization. In cDDR5-based vaccine development, it is very important to determine whether anti-cDDR antibody-producing B-cells could be reactivated when the CCR5-incorporated viruses invade the body. As shown in Fig. 3A, the epitopes of anti-rcDDR5 antibodies are likely to be effectively exposed on the surface of SIV_{mac239}. This result may support our hypothesis. Thus, these results suggest that the UPA in CCR5 is an attractive target for immune strategies aimed at reproducing the immune response in a subset of long-term non-progressors with anti-CCR5 antibodies.

Acknowledgment

We thank Dr. H. Akari (Tsukuba Primate Research Center, National Institute of Biomedical Innovation) for providing the HSC-F cells.

References

[1] M. Dean, M. Carrington, C. Winkler, G.A. Huttley, M.W. Smith, R. Allikmets, J.J. Goedert, S.P. Buchbinder, E. Vittinghoff, E. Gomperts, S. Donfield, D. Vlahov, R. Kaslow, A. Saah, C. Rinaldo, R. Detels, S.J. O'Brien, Genetic restriction of HIV-1 infection and progression to AIDS by a deletion allele of the CKR5 structural gene. Hemophilia Growth and Development Study, Multicenter AIDS Cohort Study Multicenter Hemophilia Cohort Study, San Francisco City Cohort, ALIVE Study, Science 273 (1996) 1856–1862.

[2] H. Deng, R. Liu, W. Ellmeier, S. Choe, D. Unutmaz, M. Burkhart, P. Di Marzio, S. Marmon, R.E. Sutton, C.M. Hill, C.B. Davis, S.C. Peiper, T.J. Schall, D.R. Littman, N.R. Landau, Identification of a major co-receptor for primary isolates of HIV-1, Nature 381 (1996) 661–666.

[3] C. Barassi, A. Lazzarin, L. Lopalco, CCR5-specific mucosal IgA in saliva and genital fluids of HIV-exposed seronegative subjects, Blood 104 (2004) 2205–2206.

[4] S. Misumi, R. Nakajima, N. Takamune, S. Shoji, A cyclic dodecapeptide-multiple-antigen peptide conjugate from the undecapeptidyl arch (from Arg(168) to Cys(178)) of extracellular loop 2 in CCR5 as a novel human immunodeficiency virus type 1 vaccine, J. Virol. 75 (2001) 11614–11620.

[5] S. Misumi, D. Nakayama, M. Kusaba, T. Iiboshi, R. Mukai, K. Tachibana, T. Nakasone, M. Umeda, H. Shibata, M. Endo, N. Takamune, S. Shoji, Effects of immunization with CCR5-based cycloimmunogen on simian/HIVSF162P3 challenge, J. Immunol. 176 (2006) 463–471.

[6] B. Chackerian, D.R. Lowy, J.T. Schiller, Induction of autoantibodies to mouse CCR5 with recombinant papillomavirus particles, Proc. Natl. Acad. Sci. USA 96 (1999) 2373–2378.

[7] B. Chackerian, L. Briglio, P.S. Albert, D.R. Lowy, J.T. Schiller, Induction of autoantibodies to CCR5 in macaques and subsequent effects upon challenge with an R5-tropic simian/human immunodeficiency virus, J. Virol. 78 (2004) 4037–4047.

[8] T. Lehner, C. Doyle, Y. Wang, K. Babaahmady, T. Whittall, L. Tao, L. Bergmeier, C. Kelly, Immunogenicity of the extracellular domains of C-C chemokine receptor 5 and the in vitro effects on simian immunodeficiency virus or HIV infectivity, J. Immunol. 166 (2001) 7446–7455.

[9] K. Monde, Y. Maeda, Y. Tanaka, S. Harada, K. Yusa, Gp120 V3-dependent impairment of R5 HIV-1 infectivity due to virion-incorporated CCR5, J. Biol. Chem. 282 (2007) 36923–36932.

[10] D.E. Ott, Potential roles of cellular proteins in HIV-1, Rev. Med. Virol. 12 (2002) 359–374.

[11] M.J. Tremblay, J.F. Fortin, R. Cantin, The acquisition of host-encoded proteins by nascent HIV-1, Immunol. Today 19 (1998) 346–351.

[12] D.E. Ott, Cellular proteins in HIV virions, Rev. Med. Virol. 7 (1997) 167–180.

[13] L.B. Lallos, S. Laal, J.A. Hoxie, S. Zolla-Pazner, J.C. Bandres, Exclusion of HIV coreceptors CXCR4, CCR5, and CCR3 from the HIV envelope, AIDS Res. Hum. Retroviruses 15 (1999) 895–897.

[14] H. Akari, T. Fukumori, S. Iida, A. Adachi, Induction of apoptosis in herpesvirus saimiri-immortalized T lymphocytes by blocking interaction of CD28 with CD80/CD86, Biochem. Biophys. Res. Commun. 263 (1999) 352–356.

[15] U.K. Laemmli, Cleavage of structural proteins during the assembly of the head of bacteriophage T4, Nature 227 (1970) 680–685.

[16] J. Gosling, F.S. Monteclaro, R.E. Atchison, H. Arai, C.L. Tsou, M.A. Goldsmith, I.F. Charo, Molecular uncoupling of C-C chemokine receptor 5-induced chemotaxis and signal transduction from HIV-1 coreceptor activity, Proc. Natl. Acad. Sci. USA 94 (1997) 5061–5066.

[17] S.J. Siciliano, S.E. Kuhmann, Y. Weng, N. Madani, M.S. Springer, J.E. Lineberger, R. Danzeisen, M.D. Miller, M.P. Kavanaugh, J.A. DeMartino, D. Kabat, A critical site in the core of the CCR5 chemokine receptor required for binding and infectivity of human immunodeficiency virus type 1, J. Biol. Chem. 274 (1999) 1905–1913.

[18] D. Gibellini, F. Vitone, E. Gori, M. La Placa, M.C. Re, Quantitative detection of human immunodeficiency virus type 1 (HIV-1) viral load by SYBR green real-time RT-PCR technique in HIV-1 seropositive patients, J. Virol. Methods 115 (2004) 183–189.

[19] M. Ui, T. Kuwata, T. Igarashi, K. Ibuki, Y. Miyazaki, I.L. Kozyrev, Y. Enose, T. Shimada, H. Uesaka, H. Yamamoto, T. Miura, M. Hayami, Protection of macaques against a SHIV with a homologous HIV-1 Env and a pathogenic SHIV-89.6P with a heterologous Env by vaccination with multiple gene-deleted SHIVs, Virology 265 (1999) 252–263.

[20] M. Farzan, T. Mirzabekov, P. Kolchinsky, R. Wyatt, M. Cayabyab, N.P. Gerard, C. Gerard, J. Sodroski, H. Choe, Tyrosine sulfation of the amino terminus of CCR5 facilitates HIV-1 entry, Cell 96 (1999) 667–676.

[21] N. Bannert, S. Craig, M. Farzan, D. Sogah, N.V. Santo, H. Choe, J. Sodroski, Sialylated O-glycans and sulfated tyrosines in the NH_2-terminal domain of CC chemokine receptor 5 contribute to high affinity binding of chemokines, J. Exp. Med. 194 (2001) 1661–1673.

[22] R. Liu, W.A. Paxton, S. Choe, D. Ceradini, S.R. Martin, R. Horuk, M.E. MacDonald, H. Stuhlmann, R.A. Koup, N.R. Landau, Homozygous defect in HIV-1 coreceptor accounts for resistance of some multiply-exposed individuals to HIV-1 infection, Cell 86 (1996) 367–377.

[23] M. Samson, F. Libert, B.J. Doranz, J. Rucker, C. Liesnard, C.M. Farber, S. Saragosti, C. Lapoumeroulie, J. Cognaux, C. Forceille, G. Muyldermans, C. Verhofstede, G. Burtonboy, M. Georges, T. Imai, S. Rana, Y. Yi, R.J. Smyth, R.G. Collman, R.W. Doms, G. Vassart, M. Parmentier, Resistance to HIV-1 infection in caucasian individuals bearing mutant alleles of the CCR-5 chemokine receptor gene, Nature 382 (1996) 722–725.

[24] C. Pastori, B. Weiser, C. Barassi, C. Uberti-Foppa, S. Ghezzi, R. Longhi, G. Calori, H. Burger, K. Kemal, G. Poli, A. Lazzarin, L. Lopalco, Long-lasting CCR5 internalization by antibodies in a subset of long-term nonprogressors: a possible protective effect against disease progression, Blood 107 (2006) 4825–4833.

[25] P.J. Klasse, Q.J. Sattentau, Occupancy and mechanism in antibody-mediated neutralization of animal viruses, J. Gen. Virol. 83 (2002) 2091–2108.

[26] P.W. Parren, D.R. Burton, The antiviral activity of antibodies in vitro and in vivo, Adv. Immunol. 77 (2001) 195–262.

INSTITUT PASTEUR

ELSEVIER

Microbes and Infection 10 (2008) 143–150

www.elsevier.com/locate/micinf

Original article

HIV-1 production is specifically associated with human NMT1 long form in human NMT isozymes

Nobutoki Takamune, Kayoko Gota, Shogo Misumi, Kenzo Tanaka, Shigetaka Okinaka, Shozo Shoji*

Department of Pharmaceutical Biochemistry, Faculty of Medical and Pharmaceutical Sciences, Kumamoto University, 5-1 Oe-Honmachi, Kumamoto 862-0973, Japan

Received 29 August 2007; accepted 28 October 2007
Available online 5 November 2007

Abstract

The *N*-myristoylation of the N-terminal of human immunodeficiency virus type-1 (HIV-1) $Pr55^{gag}$ by human *N*-myristoyltransferase (hNMT) is a prerequisite modification for HIV-1 production. hNMT consists of multiple isozymes encoded by *hNMT1* and *hNMT2*. The hNMT1 isozyme consists of long, medium, and short forms. Here, we investigated which isozyme is crucial for HIV-1 production. Human embryonic kidney (HEK) 293 cells transfected with infectious HIV-1 vectors were used as models of HIV-1-infected cells in this study. The significant reduction in HIV-1 production and the failure of the specific localization of $Pr55^{gag}$ in a detergent-resistant membrane fraction were dependent on the knockdown of the different forms of the hNMT1 isozyme but not of the hNMT2 isozyme. Additionally, the coexpression of an inactive mutant hNMT1 isozyme, namely the hNMT1 long form ($hNMT1_L$), but not that of other hNMT mutants resulted in a significant reduction in HIV-1 production. These results strongly suggest that HIV-1 production is specifically associated with hNMT1, particularly $hNMT1_L$, but not with hNMT2 *in vivo*, contributing to the understanding of a step in HIV-1 replication.

Keywords: *N*-Myristoyltransferase; Human immunodeficiency virus type-1

1. Introduction

N-Myristoyltransferase (NMT) (EC 2.3.1.9.7) mainly catalyzes the covalent attachment of myristate from myristoyl coenzyme A to the α-amino group of N-terminal Gly of nascent or proteolytic processed proteins [1–3]; this modification is called protein *N*-myristoylation [4]. *N*-Myristoylation is important as a main membrane-targeting signal of modified proteins [5]. The consensus sequence of peptide substrates for NMT is generally Gly-X-X-X-Ser/Thr, in which N-terminal Gly is absolutely required and Ser/Thr at position five is preferred [1,2].

N-Myristoylation is essential for modified proteins to function appropriately. Many viral proteins in addition to cellular proteins can be *N*-myristoylated [6]. *N*-Myristoylation occurs in products from the human immunodeficiency virus type-1 (HIV-1) genome: the N-terminal Gly of $Pr55^{gag}$ [7–9] and Nef [10]. $Pr55^{gag}$ is a structural protein of HIV-1 and *N*-myristoylation of $Pr55^{gag}$ is essential for the release of HIV-1 virions and HIV-1 infectivity [7–9,11,12]. The *N*-myristoyl group promotes the targeting of $Pr55^{gag}$ to the plasma membrane, particularly the detergent-resistant membrane (DRM), which is thought to be closely associated with $Pr55^{gag}$ assembly, followed by the budding of infectious viral particles [13–15].

Mammalian NMTs, particularly those in humans, mice, rats, and bovine, appear to be encoded by two genes: *NMT1* and *NMT2* [16–18]. Furthermore, human NMT1 (hNMT1) consists of at least three isozymes, namely, the hNMT1 long form ($hNMT1_L$), hNMT1 medium form ($hNMT1_M$), and hNMT1 short form ($hNMT1_S$); these isozymes were suggested to be produced by splice variants and to differ in translation start site [19,20]. Recently, it has been suggested that each

* Corresponding author. Tel.: +81 96 371 4362; fax: +81 96 362 7800.
E-mail address: shoji@gpo.kumamoto-u.ac.jp (S. Shoji).

1286-4579/$ - see front matter © 2007 Elsevier Masson SAS. All rights reserved.
doi:10.1016/j.micinf.2007.10.015

of the mouse NMT isozymes (mNMT1 and mNMT2) has different roles during mouse development [21]. However, it remains unclarified which isozyme catalyzes which substrate *in vivo*. Thus, it is important to understand which isozyme is closely associated with the HIV-1 life cycle, because the isozyme involved in HIV-1 replication could be used as a specific target in host factors for the development of anti-HIV-1 agents that are effective for evasive drug-resistant viruses. In this study, we tried to determine which hNMT isozyme plays a crucial role in HIV-1 production in which the *N*-myristoylation of $Pr55^{gag}$ is involved.

2. Materials and methods

2.1. Materials

HEK293 cells, infectious HIV-1 expression vectors pNL4-3, pYU-2, pYK-JRCSF, and p89.6 were obtained from the NIH AIDS Research & Reference Reagent Program. Dulbecco's modified Eagle's medium (DMEM) and RPMI 1640 medium were obtained from Nissui Pharmaceutical Co. Ltd.

2.2. Cell culture

HEK293 cells were cultured at 37 °C in DMEM supplemented with 10% heat-inactivated fetal calf serum containing 100 IU/ml penicillin and 100 μg/ml streptomycin in 5% CO_2

2.3. Double-stranded RNAs

The target sequences of double-stranded RNAs (dsRNAs) inducing RNAi against hNMT1 and hNMT2 were 5′-GCGAC CAATGGAAACAAAGGACATT-3′ and 5′-GCTCAAGGAG TTATACACGTTGTTA-3′, respectively. dsRNA with a nonspecific randomized sequence was used for the control experiments. dsRNAs were prepared as Stealth™ RNAi (Invitrogen, Carlsbad, CA).

2.4. Cell growth assay

HEK293 cells (4.0×10^4 cells) were cultured in 96-well plates overnight. The cells were transfected with 0, 3.1, 6.1, 12.5, 25, 50, and 100 pmol/ml siRNAs using Lipofectamine 2000 and cultured for 48 h. The cell viability was evaluated by WST-1 method [28]. The cell transfected with or without 10 pmol/ml of siRNAs were visually inspected by microscopy and photographed (×100).

2.5. Reverse transcription and semiquantitative real-time polymerase chain reaction (PCR)

Total RNA was extracted using ISOGEN (Nippon Gene Co. Ltd., Tokyo, Japan) according to the manufacturer's instruction. First-strand cDNA synthesis was performed using the SuperScript™ III First-Strand Synthesis System for RT–PCR (Invitrogen, Carlsbad, CA) according to the manufacturer's instruction, in which oligo $(dT)_{20}$ was used as a primer. DyNAmo™ HS SYBR®Green qPCR kit (Finnzymes, Espoo, Finland) reagents were used as semiquantitative real-time PCR reagents according to the manufacturer's instruction. Thermocycling was carried out using the DNA Engine Opticon®2 System (MJ Research Inc., Waltham, MA). The oligonucleotide primers used for the PCR were as follows: hNMT1 sense primer, CCGCAGATGATGGAAGGGAA; hNMT1 antisense primer, CCTCTCTGCTGGCAAAGAGTTCA; hNMT2 sense primer, GAAGTCCTGGAGGGTATTTG; hNMT2 antisense primer, CTGCATTGGAACACTGGGATT; β-actin sense primer, CGGAACCGCTCATTGCC; β-actin antisense primer, ACCCACATCGTGCCCATCTA.

2.6. Construction of each hNMT isozyme expression vector

Total RNA was extracted from CEM cells, a human T-cell line, using a QuickPrep Total RNA Extraction kit (Amersham Biosciences Corp, Piscataway, NJ) according to the manufacturer's instruction. First-strand cDNAs were obtained by the reverse transcription of total RNA using a Gene Amp RNA PCR kit (Applied Biosystems, Foster City, CA). The cDNA of each hNMT isozyme was amplified by PCR with *pfu* Turbo Hotstart DNA polymerase (Stratagene, La Jolla, CA) using a primer pair on the basis of the reported GenBank accession numbers: BC006569 for hNMT1 and AF043325 for hNMT2. The sequences of primers used for the construction of each hNMT isozyme expression vector in mammalian cells were as follows: CATGAATTCATGGCGGACGAGAGTGAGAC with the 5′-EcoRI restriction site for $hNMT1_L$ as the sense primer; CATGAATTCATGGAAGGGAACGGGAACGGC CATG with the 5′-EcoRI restriction site for $hNMT1_M$ as the sense primer; CATGAATTCATGAACTCTTTGCCAGCA GAG with the 5′-EcoRI restriction site for $hNMT1_S$ as the sense primer; CATCTCGAGTTATTGTAGCACCAGTC CAAC with the 5′-XhoI restriction site for all the hNMT1 isozymes as the antisense primer; CATGAATTCATGGCG GAGGACAGCGAGTC with the 5′-EcoRI restriction site for hNMT2 as the sense primer; and CATCTCGAGCTATTG TAGTACTAGTCCAAC with the 5′-XhoI restriction site for hNMT2 as the antisense primer. Each hNMT isozyme cDNA amplified by PCR was subcloned into the pT7Blue vector (Merck KGaA, Darmstadt, Germany) according to the manufacturer's instruction. Each cDNA digested with EcoRI and XhoI was cloned into the pcDNA4/HisMax vector (Invitrogen) for its expression in mammalian cells.

2.7. Site-directed mutagenesis for Gly^{412} to Lys^{412} mutation of each hNMT isozyme

The sequences of the primers used for the site-directed mutagenesis of each hNMT isozyme expression vector were as follows: CAGAGAAGGTTAAACTGGTGCTACAATAAC for the hNMT1 isozyme mutation sense primer; GTAGCAC CAGTTTAACCTTCTCTGCCCCC for the hNMT1 isozyme mutation antisense primer; CTGAAAAGGTTAAACTAG TACTACAATAG for the hNMT2 mutation sense primer; and

GTAGTACTAGTTTAACCTTTTCAGAATCTG for the hNMT2 mutation antisense primer. The mutations were induced using a QuikChange site-directed mutagenesis kit (Stratagene) according to the instruction manual.

2.8. Quantification of HIV-1 p24 antigen in supernatant

HEK293 cells (1.0×10^5 cells) were cultured in 48-well plates overnight. Confluent cells (30–50%) were cotransfected with 10 pmol of dsRNAs and HIV-1 expression vectors (pNL4-3, pYU-2, pYK-JRCSF, or p89.6) using Lipofectamine2000. Alternatively, HEK293 cells (3.0×10^5 cells) were cultured in 24-well plates overnight. The cells were transfected with a plasmid expressing each Xpress™ epitope-tagged hNMT isozyme ($hNMT1_L$, $hNMT1_M$, $hNMT1_S$, and hNMT2) or a comparable inactive form, whose plasmids are described in detail below, using Lipofectamine2000, and then transfected with pNL4-3 after 24 h. After 24 h or 48 h of further cultivation, the supernatant was collected and centrifuged to remove cell debris. The amount of HIV-1 p24 antigen in the cell-free supernatant was measured using an enzyme-linked immunosorbent assay (ELISA) kit (ZeptoMetrix Corp., Buffalo, NY) according to the manufacturer's instruction.

2.9. Cell lysis and Western immunoblot analysis

The cells were washed twice with phosphate-buffered saline, lysed in the lysis buffer, and subjected to sodium dodecyl sulfate–polyacrylamide gel electrophoresis (SDS–PAGE) and Western blot analysis [27]. The serum and antibodies used in different immunoblottings were as follows: HIV-1-positive plasma (a gift from Dr. Shuzo Matsushita of Kumamoto University, AIDS Research Institute, Kumamoto, Japan), actin (Ab-1) kit (Oncogene Research Products, Boston, MA), anti-Xpress™ antibody (Invitrogen), anti-caveolin-1 (Sigma, St. Louis, MO), anti-transferrin receptor (BD Pharmingen, San Diego, CA), anti-NMT1 (BD Pharmingen), and anti-NMT2 (BD Pharmingen). Immune complexes were detected with appropriate peroxidase-conjugated secondary antibodies followed by visualization by chemiluminescence detection (NEN Life Science Products, Boston, MA).

2.10. Flotation assay and Western blot analysis

Flotation assay was performed as previously described [22]. The final five fractions were prepared from the top to the bottom of the tube and subjected to SDS–PAGE and Western immunoblot analysis as described above. HIV-1 antigens were probed with HIV-1-positive plasma. The transferrin receptor and caveolin-1 were used as non-DRM and DRM markers, respectively.

3. Results

3.1. Inhibition of expressions of hNMT1 isozymes and hNMT2 by RNAi

There are two kinds of mRNA, namely, extended 5′-mRNA and alternatively spliced mRNA, in hNMT1, from which $hNMT1_L$, $hNMT1_M$, and $hNMT1_S$ could be produced [20]; however, the *hNMT2* gene produces only one protein: hNMT2 [17]. In this study, two kinds of chemically synthetic double-stranded siRNA were designed: one targets all kinds of hNMT1 mRNA and the other targets hNMT2 mRNA. siRNA with a randomized sequence was also used for the control experiments. HEK293 cells were transfected with siRNAs and cultured for 48 h. The effects of the siRNAs at doses from 0 to 100 pmol/ml on cell growth were evaluated by the WST-1 method. As shown in Fig. 1A, similar dose-dependent cytotoxic effect of siRNAs was observed in the three siRNAs. The treatment of HEK293 cells with 10 pmol/ml siRNAs, which show no cytotoxic effect, showed no change in cell morphology compared with the nontreatment of HEK293 cells (Fig. 1B). the siRNA dose of 10 pmol/ml was therefore used for the other subsequent experiments. To examine whether siRNAs knock down mRNAs specifically, HEK293 cells were transfected with siRNAs and cultured for 48 h. mRNA level was semiquantified by real-time RT–PCR analysis. β-Actin mRNA was selected as the internal standard for semiquantification. The hNMT1 and hNMT2 mRNA expression levels of HEK293 cells treated with each siRNA decreased from about 20% to 30% the expression level of each control mRNA (Fig. 1C and D, respectively). Additionally, the each specific suppression of isozyme by each siRNA was observed (Fig. 1C and D).

3.2. Failure of specific localization of $Pr55^{gag}$ in DRM with knockdown of hNMT1 isozymes

$Pr55^{gag}$ is associated with the DRM fraction during assembly in the late stage of HIV-1 replication [13,14], in which its localization is dependent on its *N*-myristoylation [13]. The effect of the knockdown of each NMT isozyme on the localization of $Pr55^{gag}$ in the DRM fraction was therefore evaluated. pNL4-3-transfected HEK293 cells were treated with siRNA directed by either hNMT1 or hNMT2, cultured and subjected to flotation assay [22]. The pNL4-3G2A mutant was used in addition to wild-type pNL4-3 in the control experiment for comparison of the localizations of non-*N*-myristoylated $Pr55^{gag}$ and *N*-myristoylated $Pr55^{gag}$. The transferrin receptor and caveolin-1 were used as the non-DRM and DRM markers, respectively. As shown in Fig. 2*N*-myristoylated $Pr55^{gag}$ in pNL4-3-transfected HEK293 cells was specifically detected in fraction 1 similarly to caveolin-1, defined as the DRM fraction, whereas a large amount of non-*N*-myristoylated $Pr55^{gag}$ in pNL4-3G2A-mutant-transfected HEK293 cells was detected, as expected, in the fraction similar to that for the transferrin receptor, defined as the non-DRM fraction. These results show that the specific localization of $Pr55^{gag}$ in DRM is

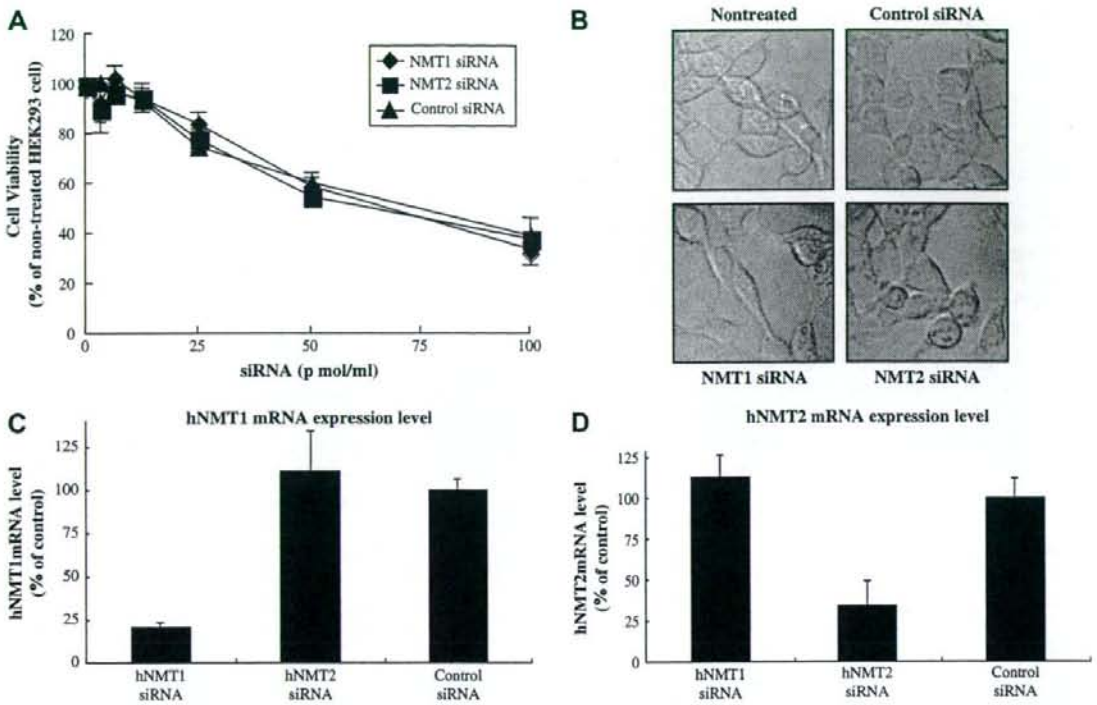

Fig. 1. Inhibition of hNMT1 and hNMT2 mRNA expressions by siRNAs in HEK293 cells. HEK293 cells were transfected with hNMT1- and hNMT2-specific siRNAs and control siRNA separately. The cells were harvested at 48 h post-transfection. The dose-dependent effect of siRNAs on cell growth was evaluated by the WST-1 method as described in Materials and methods (A). The cell morphology 48 h after transfection of each siRNA (10 pmol/ml) was visually inspected by microscopy and photographed (×100) (B). The mRNA expression levels of hNMT1 (C) and hNMT2 (D) were semiquantified by real-time PCR analysis using specific primer pairs, as described in Section 2. β-Actin mRNA level was used as the internal standard. Cell viability and mRNA expression level are expressed as percentage relative to those obtained in the siRNA-nontreated and control siRNA-treated experiments, respectively. Means and standard deviations from three independent experiments are shown.

dependent on *N*-myristoylation, as previously demonstrated [13]. By performing the same flotation assay, the localization of $Pr55^{gag}$ was examined in HEK293 cells with all the hNMT1 isozymes or hNMT2 knocked down. As shown in Fig. 2, $Pr55^{gag}$ was detected in the non-DRM fraction from the HEK293 cells with all the hNMT1 isozymes knocked down. On the other hand, $Pr55^{gag}$ was specifically detected in the DRM fraction from the HEK293 cells with hNMT2 knocked down, similarly to that observed in the control experiment.

3.3. Knockdown of hNMT1 isozymes affects HIV-1 release

Since $Pr55^{gag}$*N*-myristoylation appears to be required in the release of HIV-1 particles [11,12], the late stage of the HIV-1 life cycle must be directly involved in either or both hNMT isozymes. As control experiment, a comparison of HIV-1 production between pNL4-3 and pNL4-3G2A mutant was conducted in parallel. The production of HIV-1 with non-*N*-myristoylated $Pr55^{gag}$ was about 13% that of the wild-type HIV-1 (Fig. 3E); however, the expression levels of $Pr55^{gag}$ in HEK293 cells, which were confirmed by Western immunoblot analysis, were almost the same between the wild-type HIV-1 and the mutant HIV-1 (Fig. 3E).

The effects of siRNAs on the production of the HIV-1 progeny were evaluated, in which HEK293 cells transfected with infectious HIV-1 expression vectors, namely, pNL4-3, p89.6, pYK-JRCSF, and pYU2, were used. The amount of HIV-1 p24 antigen in the supernatant was quantified by ELISA to evaluate HIV-1 production. As shown in Fig. 3A–D, the amount of HIV-1 p24 antigen in the supernatant of cells with the hNMT1 isozymes knocked down was significantly lower than that in the supernatant of the control cells for all the HIV-1 strains tested, whereas the amount of HIV-1 p24 antigen in the supernatant of the cells with hNMT2 knocked down was the same as that in the supernatant of the control cells for all the HIV-1 strains tested. The significant reduction in HIV-1 production was dependent on the knockdown of the hNMT1 isozymes. The knockdown of the hNMT1 isozymes was sufficient to significantly decrease HIV-1 production in the experiments. Similar expression levels of $Pr55^{gag}$ as an expression product of the HIV-1 gene in the transfected cells (Fig. 3A–E), in which actin was detected as internal control, were confirmed. Taken together, the results indicate that

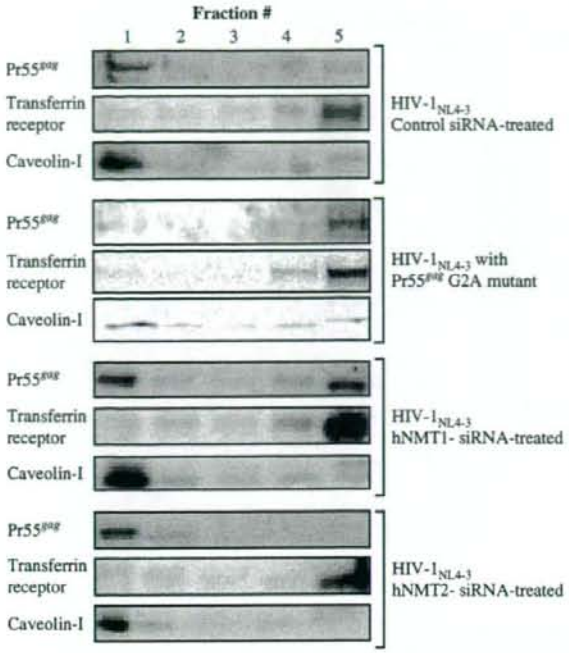

Fig. 2. Effect of knockdown of either hNMT1 or hNMT2 on localization of $Pr55^{gag}$ in DRM and non-DRM fractions. HEK293 cells were transfected with siRNA against hNMT1, hNMT2 and control as indicated at 48 h post-transfection with pNL4-3. The cells 96 h after the initial transfection were washed and subjected to flotation assay. The pNL4-3G2A mutant was used to detect the localization of non-*N*-myristoylated $Pr55^{gag}$ as the control experiment. Results of experiments involving treatment with each siRNA are shown. $Pr55^{gag}$ was detected by Western immunoblot analysis using HIV-1-positive plasma. The transferrin receptor and caveolin-1 were used as the non-DRM and DRM markers, respectively.

hNMT1 contributes to HIV-1 production more than hNMT2 in the late stage of HIV-1 replication.

3.4. Coexpression of inactive $hNMT1_L$ mutant with HIV-1 decreases HIV-1 production

As shown in Figs. 2 and 3, the results of the experiments with siRNAs strongly suggest that hNMT1 isozymes are involved in the late stage of HIV-1 replication. To determine which hNMT1 isozyme ($hNMT1_L$, $hNMT1_M$, or $hNMT1_S$) most effectively contributes to HIV-1 production, inactive mutants of the hNMT1 isozymes were used as dominant negative mutants for the evaluation. The inactive form of hNMT2 was also used as the negative control, because the knockdown experiments with hNMT2 siRNA showed no inhibitory effect on HIV-1 production (Fig. 3). Each Xpress epitope-tagged hNMT isozyme expression vector was constructed, and site-directed mutation for Gly^{412} to Lys^{412} in all the hNMT1 isozymes and hNMT2 was introduced in Section 2, in which the number corresponds to $hNMT1_S$ and the amino acid is located five residues from the *C*-terminus of each isozyme. It was previously reported that comparable mutants are inactive forms of human and yeast NMTs [16]. Each of the wild-type and mutant hNMT isozymes was separately expressed in HEK293 cells by each Xpress epitope-tagged expression vector, followed by transfection with pNL4-3. The amounts of HIV-1 p24 antigen in the supernatant 24 h and 48 h after pNL4-3 transfection were quantified by ELISA to evaluate HIV-1 production. As shown in Fig. 4A–C, the amounts of HIV-1 p24 antigen in the supernatants of $hNMT1_L$-mutant-expressing HEK293 cells 24 h and 48 h after the transfection were significantly lower than that in the supernatant of wild-type-$hNMT1_L$-expressing HEK293 cells (Fig. 4C). On the other hand, no differences between the wild type and the mutant were observed for the other hNMT1 isozymes (Fig. 4A,B). As expected, no effect of the inactive form of hNMT2 on HIV-1 production was observed (Fig. 4D). Similarities in expression level between the wild types and the mutants were observed for the respective sets of Xpress-tagged NMT isozymes studied (Fig. 4E–G). Similar expression levels of $Pr55^{gag}$ in each of the transfected cells were also observed (Fig. 4E–G). Actin was used as internal control in each sample.

As shown in Fig. 4I, endogenous NMT1 and NMT2 isozymes were detected by Western immunoblot analysis. As shown in Fig. 4I, a higher expression level of endogenous $NMT1_L$ than of other NMT1 isozymes was observed, in which endogenous $NMT1_M$ and $NMT1_S$ expressed about 30% and 15% that of $NMT1_L$, respectively.

4. Discussion

N-Myristoylation is acylation specific to N-terminal Gly in proteins, which is an important component of membrane-targeting signals in general. Many kinds of viral protein are *N*-myristoylated [6], for example, the VP4 of the poliovirus [23], the VP2 of the simian virus 40 [24], the L protein of the hepatitis B virus [25], and the $pp60^{src}$ of the Rous sarcoma virus [26] in addition to the $Pr55^{gag}$ and Nef of HIV-1. Since NMT is a common host factor for many kinds of virus, it is important to understand the detailed relationship between NMT and the replication of each virus. In this study, we focus on the relationship between HIV-1 production and each hNMT isozyme.

We hypothesize that each hNMT isozyme exclusively or predominantly catalyzes the *N*-myristoylation of specific substrate proteins *in vivo* or that each hNMT isozyme has a specific role *in vivo*. For example, $Pr55^{gag}$ could be *N*-myristoylated with a specific hNMT isozyme.

$Pr55^{gag}$ *N*-myristoylation is closely associated with HIV-1 phenotypes including the $Pr55^{gag}$ localization to the DRM fraction [13,14] and HIV-1 production [11]. $Pr55^{gag}$ *N*-myristoylation can efficiently drive $Pr55^{gag}$ to the cell membrane after translation [27] and enhance the association of $Pr55^{gag}$ with DRM [13], followed by the assembly of $Pr55^{gag}$ and the budding of viral particles [14]. The late stage of HIV-1 replication was therefore focused on to evaluate the contribution of each isozyme to the HIV-1 life cycle.

In the flotation assay, the localization of $Pr55^{gag}$ in the non-DRM fraction was observed with the knockdown of the

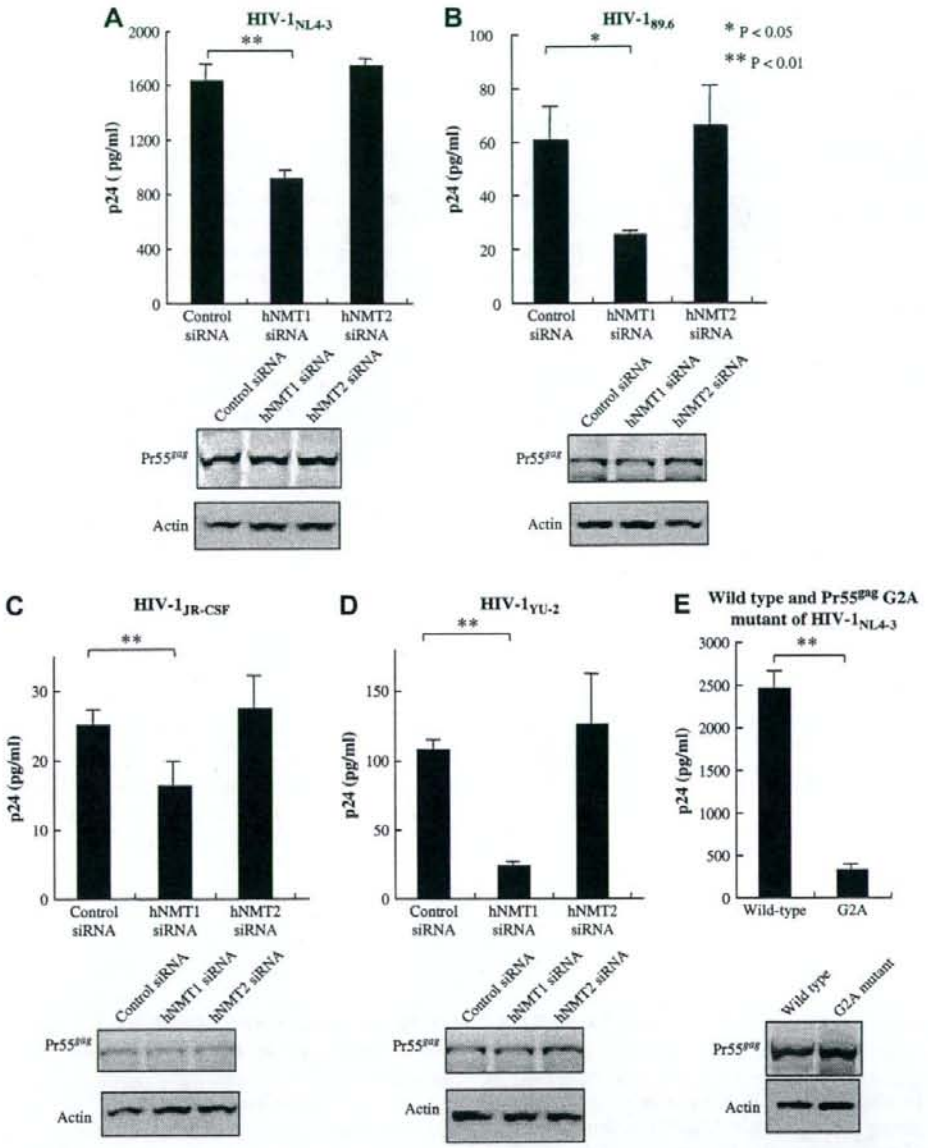

Fig. 3. Effect of knockdown of hNMT isozymes on HIV-1 production. HEK293 cells were cotransfected with siRNA and an HIV-1 expression vector. Alternatively, HEK293 cells were transfected with pNL4-3 or the pNL4-3G2A mutant. The amount of HIV-1 p24 antigen in the supernatant at 48 h post-transfection was quantified by ELISA, as described in Section 2. Each cell lysate was analyzed by Western immunoblot analysis, as described in Section 2. The expressions of $Pr55^{gag}$ as an expression product of the HIV-1 gene and actin as internal control are shown in the upper and bottom panels, respectively. (A) pNL4-3 (B) p89.6, (C) pYK-JRCSF, (D) pYU-2, (E) pNL4-3 and pNL4-3 G2A mutant. Means and standard deviations from three independent experiments are shown. *P* was calculated using Student's *t*-test. $*P < 0.05$ and $**P < 0.01$ for control siRNA vs. either hNMT1 siRNA.

hNMT1 isozymes except hNMT2 (Fig. 2). It was also shown that the significant reduction in HIV-1 production is dependent on the knockdown of the hNMT1 isozymes in all the HIV-1 strains tested (Fig. 3A–D). The results suggest that a large amount of non-*N*-myristoylated $Pr55^{gag}$ with the knockdown of all the hNMT1 isozymes but not hNMT2 localizes in the non-DRM fraction, in which no appropriate $Pr55^{gag}$ assembly occurs, resulting in a decreased HIV-1 production.

Overall, the reduction rate of the p24 antigen of each viral strain in the supernatant by hNMT1 siRNA (Fig. 3) was less than that of hNMT mRNA by hNMT1 siRNA (Fig. 1C). These results seem reasonable, because even if $Pr55^{gag}$ was not *N*-myristoylated by

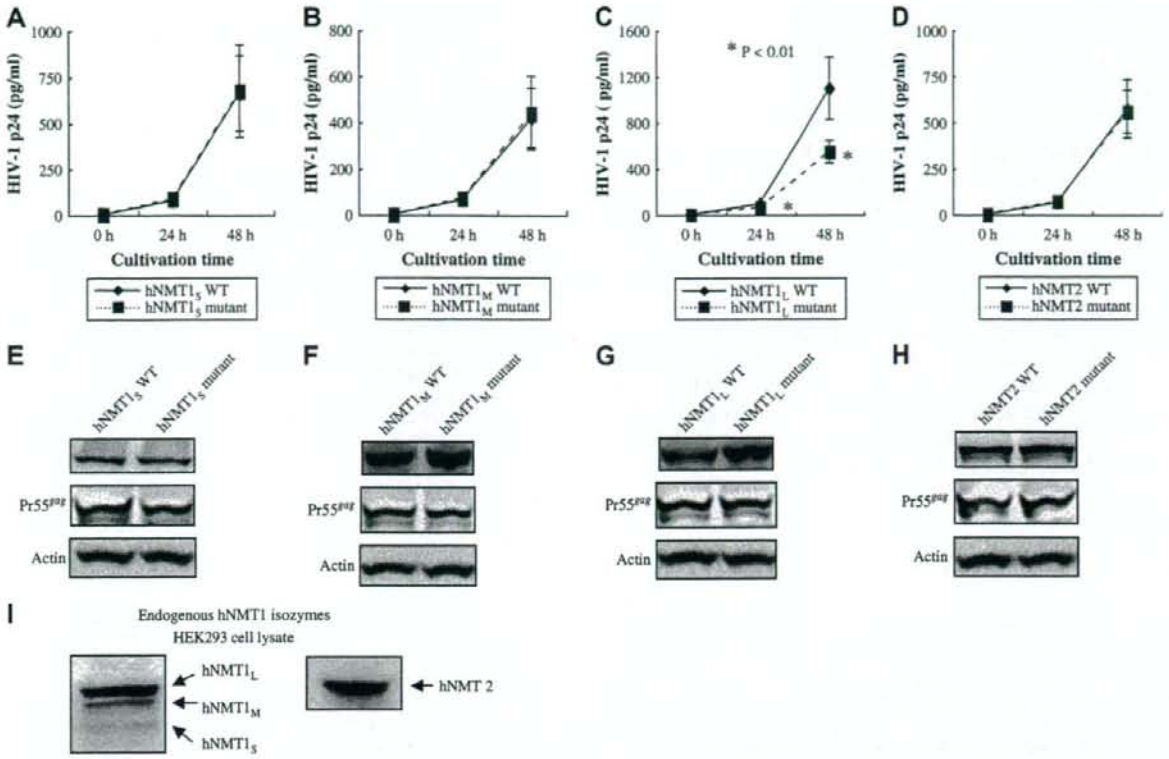

Fig. 4. Effect of each inactive hNMT isozyme mutant on HIV-1 production. HEK293 cells were transfected with a plasmid expressing each Xpress™ epitope-tagged hNMT isozyme (hNMT1$_L$, hNMT1$_M$, hNMT1$_S$, and hNMT2) or a comparable inactive form, followed by transfection with pNL4-3 after 24 h. The amount of HIV-1 p24 antigen in the supernatant 24 h and 48 h after transfection with pNL4-3 was quantified by ELISA, as described in Section 2 (A–D). Each cell lysate 48 h after transfection was analyzed by Western immunoblot analysis, as described in Section 2. The expressions of each Xpress-tagged NMT isozyme, Pr55^{gag} as an expression product of the HIV-1 gene, and actin as internal control are shown in the upper, middle, and bottom panels, respectively (E–H). Nontreated HEK293 cell lysate was subjected to SDS–PAGE and Western immunoblot analysis to detect endogenous NMT1 and NMT2 using anti-NMT1 and anti-NMT2, respectively, as described in Section 2 (I). Means and standard deviations from four independent experiments are shown for the ELISA results. P was calculated using Student's t-test. *$P < 0.01$ for active form vs. comparable inactive form after 24 h or 48 h of cultivation.

the G2A mutation of the amino terminus, the reduction rate of the p24 antigen was not 100% but about 90% (Fig. 3E).

The evaluation of the dominant negative effect exerted by the inactive form of each hNMT1 isozyme on HIV-1 production resulted in a significant reduction in HIV-1 production by the hNMT1$_L$ mutant (Fig. 4C). It is thought that the mutant hNMT1$_L$ partly competed with endogenous hNMT1$_L$ for substrate proteins including Pr55^{gag}, whereas the mutants of hNMT1$_S$, hNMT1$_M$, and hNMT2 competed with their corresponding endogenous forms for substrate proteins excluding Pr55^{gag}.

Since a higher expression level of endogenous hNMT1$_L$ than of other hNMT1 isozymes was observed in HEK293 cells (Fig. 4I), the dominant negative effect of the mutant seems to attenuate. Additionally, the difference in viral production between the coexpression of wild-type hNMT1$_L$ and that of the mutant might have resulted from the sum of the suppression of HIV-1 production by the mutant and the enhancement of HIV-1 production by the wild-type hNMT1$_L$.

It should be considered that hNMT1$_L$ disruption could affect not only the Pr55^{gag} function but also the functions of some cellular substrate proteins, which could lead to the inhibition of HIV-1 production. Although it is extremely difficult to comprehensively understand at this point which substrate proteins of hNMT1$_L$ are involved *in vivo*, at least Pr55^{gag} is the likely substrate of hNMT1$_L$ *in vivo*. At the same time, it could be expected that hNMT1$_L$ disruption could not affect the functions of substrate proteins associated with hNMT1$_S$, hNMT1$_M$, and hNMT2 *in vivo*.

Interestingly, it appeared that recombinant hNMT1 and hNMT2 could catalyze the *N*-myristoylation of peptide substrates derived from Pr55^{gag} according to the results of the *in vitro* experiments (data not shown). It is therefore suggested that the affinity between hNMT1 and the N-terminal amino acid sequence of Pr55^{gag} is not the only determinant for the exclusive hNMT1 utilization by Pr55^{gag} *in vivo*.

Altogether, the results suggest that hNMT1$_L$ is specifically associated with the late stage of HIV-1 replication *in vivo*. The contribution of our study to progress in this research area is the clarification of the hNMT isozyme that could be a more specific target molecule for the development of anti-HIV-1 agents

that could inhibit the DRM localization of $Pr55^{gag}$. Additionally, results of our study suggest that each hNMT isozyme has a specific role *in vivo*, from which an interesting question arises: "What is the mechanism underlying the specific role of each hNMT isozyme *in vivo*?" Answers to this question and others are expected to contribute to the development of not only novel anti-HIV strategies but also strategies against other pathogenic viruses with *N*-myristoylation.

Acknowledgments

We thank Dr. S. Matsushita (Kumamoto University, AIDS Research Institute, Kumamoto, Japan) for providing the HIV-1-positive plasma. This study was supported in part by a Grant-in-Aid for Scientific Research from the Ministry of Education, Culture, Sports, Science and Technology of Japan, and a Health Science Research Grant from the Ministry of Health, Labour, and Welfare of Japan.

References

[1] D.A. Towler, S.P. Adams, S.R. Eubanks, D.S. Towery, E. Jackson-Machelski, L. Glaser, J.I. Gordon, Myristoyl CoA:protein N-myristoyltransferase activities from rat liver and yeast possess overlapping yet distinct peptide substrate specificities, J. Biol. Chem. 263 (1988) 1784–1790.

[2] D.A. Towler, L. Glaser, Protein fatty acid acylation: enzymatic synthesis of an N-myristoylglycyl peptide, Proc. Natl. Acad. Sci. U.S.A. 83 (1986) 2812–2816.

[3] J. Zha, S. Weiler, K.J. Oh, M.C. Wei, S.J. Korsmeyer, Posttranslational N-Myristoylation of BID as a molecular switch for targeting mitochondria and apoptosis, Science 290 (2000) 1761–1765.

[4] S.A. Carr, K. Biemann, S. Shoji, D.C. Parmelee, K. Titani, n-Tetradecanoyl is the NH2-terminal blocking group of the catalytic subunit of cyclic AMP-dependent protein kinase from bovine cardiac muscle, Proc. Natl. Acad. Sci. U.S.A. 79 (1982) 6128–6131.

[5] M.D. Resh, Fatty acylation of proteins: new insights into membrane targeting of myristoylated and palmitoylated proteins, Biochim. Biophys. Acta. 1451 (1999) 1–16.

[6] J.A. Boutin, Myristoylation, Cell Signal 9 (1997) 15–35.

[7] R.J. Mervis, N. Ahmad, E.P. Lillehoj, M.G. Raum, F.H. Salazar, H.W. Chan, S. Venkatesan, The gag gene products of human immunodeficiency virus type 1: alignment within the gag open reading frame, identification of posttranslational modifications, and evidence for alternative gag precursors, J. Virol. 62 (1988) 3993–4002.

[8] S. Shoji, A. Tashiro, Y. Kubota, Antimyristoylation of gag proteins in human T-cell leukemia and human immunodeficiency viruses with N-myristoyl glycinal diethylacetal, J. Biochem. 103 (1988) 747–749.

[9] F.D. Veronese, T.D. Copeland, S. Oroszlan, R.C. Gallo, M.G. Sarngadharan, Biochemical and immunological analysis of human immunodeficiency virus gag gene products p17 and p24, J. Virol. 62 (1988) 795–801.

[10] B. Guy, M.P. Kieny, Y. Riviere, C. Le Peuch, K. Dott, M. Girard, L. Montagnier, J.P. Lecocq, HIV F/3′ orf encodes a phosphorylated GTP-binding protein resembling an oncogene product, Nature 330 (1987) 266–269.

[11] M. Bryant, L. Ratner, Myristoylation-dependent replication and assembly of human immunodeficiency virus 1, Proc. Natl. Acad. Sci. U.S.A. 87 (1990) 523–527.

[12] K.H. Furuishi, M. MatsuokaTakama, I. Takahashi, S. Misumi, S. Shoji, Blockage of N-myristoylation of HIV-1 gag induces the production of impotent progeny virus, Biochem. Biophys. Res. Commun. 237 (1997) 504–511.

[13] L. Ding, A. Derdowski, J.-J. Wang, P. Spearman, Independent segregation of human immunodeficiency virus type 1 Gag protein complexes and lipid rafts, J. Virol. 77 (2003) 1916–1926.

[14] A. Ono, E.O. Freed, Plasma membrane rafts play a critical role in HIV-1 assembly and release, Proc. Natl. Acad. Sci. U.S.A. 98 (2001) 13925–13930.

[15] A. Tashiro, S. Shoji, Y. Kubota, Antimyristoylation of the gag proteins in the human immunodeficiency virus-infected cells with N-myristoyl glycinal diethylacetal resulted in inhibition of virus production, Biochem. Biophys. Res. Commun. 165 (1989) 1145–1154.

[16] R.J. Duronio, S.I. Reed, J.I. Gordon, Mutations of human myristoyl-CoA:protein N-myristoyltransferase cause temperature-sensitive myristic acid auxotrophy in Saccharomyces cerevisiae, Proc. Natl. Acad. Sci. U.S.A. 89 (1992) 4129–4133.

[17] D.K. Giang, B.F. Cravatt, A second mammalian N-myristoyltransferase, J. Biol. Chem. 273 (1998) 6595–6598.

[18] V. Rioux, E. Beauchamp, F. Pedrono, S. Daval, D. Molle, D. Catheline, P. Legrand, Identification and characterization of recombinant and native rat myristoyl-CoA:protein N-myristoyltransferases, Mol. Cell Biochem. 286 (2006) 161–170.

[19] C.J. Glover, K.D. Hartman, R.L. Felsted, Human N-myristoyltransferase amino-terminal domain involved in targeting the enzyme to the ribosomal subcellular fraction, J. Biol. Chem. 272 (1997) 28680–28689.

[20] R.A. McIlhinney, K. Young, M. Egerton, R. Camble, A. White, M. Soloviev, Characterization of human and rat brain myristoyl-CoA: protein N-myristoyltransferase: evidence for an alternative splice variant of the enzyme, Biochem. J. 333 (1998) 491–495.

[21] S.H. Yang, A. Shrivastav, C. Kosinski, R.K. Sharma, M.H. Chen, L.G. Berthiaume, L.L. Peters, P.T. Chuang, S.G. Young, M.O. Bergo, N-Myristoyltransferase 1 is essential in early mouse development, J. Biol. Chem. 282 (2005) 18990–18995.

[22] S. Manes, E. Mira, C. Gomez-Mouton, R.A. Lacalle, P. Keller, J.P. Labrador, C. Martinez-A, Membrane raft microdomains mediate front-rear polarity in migrating cells, EMBO J. 18 (1999) 6211–6220.

[23] A.V. Paul, A. Schultz, S.E. Pincus, S. Oroszlan, E. Wimmer, Capsid protein VP4 of poliovirus is *N*-myristoylated, Proc. Natl. Acad. Sci. U.S.A. 84 (1999) 7827–7831.

[24] C.H. Streuli, B.E. Griffin, Myristic acid is coupled to a structural protein of polyoma virus and SV40, Nature 326 (1987) 619–622.

[25] P. Gripon, J. Le Seyec, S. Rumin, C. Guguen-Guillouzo, Myristoylation of the hepatitis B virus large surface protein is essential for viral infectivity, Virology 213 (1995) 292–299.

[26] A.M. Schultz, L.E. Henderson, S. Oroszlan, E.A. Garber, H. Hanafusa, Amino terminal myristoylation of the protein kinase p60src, a retroviral transforming protein, Science 227 (1985) 427–429.

[27] T. Shiraishi, S. Misumi, M. Takama, I. Takahashi, S. Shoji, Myristoylation of human immunodeficiency virus type 1 gag protein is required for efficient env protein transportation to the surface of cells, Biochem. Biophys. Res. Commun. 282 (2001) 1201–1205.

[28] M. Ishiyama, M. Shiga, K. Sakamoto, M. Mizoguchi, P.-G. He, A new sulfonated tetrazolium salt that produces a highly water-soluble formazan dye, Chem. Pharm. Bull. 41 (1993) 1118–1122.